Targeting the IRE1α/XBP1 Signaling Axis Suppresses Rhabdomyosarcoma Growth and Promotes Myogenic Differentiation

Anh Tuan Vuong[1,2], Aniket S Joshi[1,2], Phuong T. Ho[1,2], Meiricris Tomaz da Silva[1,2], Bin Guo[1,2], Meghana V. Trivedi[1,3], and Ashok Kumar[1,2,#]

[1]Institute of Muscle Biology and Cachexia, University of Houston College of Pharmacy, Houston, TX 77204, USA.

[2]Department of Pharmacological and Pharmaceutical Sciences, University of Houston College of Pharmacy, Houston, TX 77204, USA

[3]Department of Pharmacy Practice and Translational Research, University of Houston College of Pharmacy, Houston, TX 77204, USA

[#]Corresponding author:
Ashok Kumar, Ph.D.
Institute of Muscle Biology and Cachexia
Department of Pharmacological and Pharmaceutical Sciences
Health Building 2, Room 5012
College of Pharmacy
University of Houston
Houston, TX 77204-1217

Phone: 713-743-3376
Email: akumar43@Central.UH.EDU

Running title: Role of IRE1α/XBP1 axis in rhabdomyosarcoma

Key words: ER stress, IRE1α, unfolded protein response, Rhabdomyosarcoma, and BMP signaling.

Declaration of interest. The authors declare no competing interests.

Funding. This work was supported by the National Institute of Health grant CA294365 and AR081487 to AK.

ABSTRACT

Rhabdomyosarcoma (RMS) is the most common and aggressive pediatric soft tissue sarcoma arising from skeletal muscle lineage. Despite multimodal therapy, treatment options for relapsed or refractory RMS remain limited, highlighting the need for new therapeutic targets. The unfolded protein response (UPR) maintains cellular proteostasis under endoplasmic reticulum (ER) stress, with the inositol-requiring enzyme 1α (IRE1α)-X-box binding protein 1 (XBP1) axis serving as a key regulatory branch. While aberrant IRE1α/XBP1 signaling has been implicated in several cancers, its role in RMS is unknown. Here, we show that the IRE1α/XBP1 pathway is highly activated in both embryonal and alveolar RMS cell lines, as well as in patient tumor specimens. Genetic or pharmacological inhibition of IRE1α/XBP1pathway suppresses cell proliferation, enhances chemosensitivity, and promotes terminal differentiation in RMS cells. Moreover, IRE1α/XBP1 inhibition reduces the cancer stem cell population and suppresses the epithelial-to-mesenchymal transition phenotype. The IRE1α/XBP1 signaling drives RMS progression through XBP1-mediated upregulation of *BMPR1A*, leading to the activation of BMP-Smad1 signaling. In addition, inducible knockdown of XBP1 significantly attenuates RMS tumor growth in xenograft mouse models. Similarly, inhibition of IRE1α activity using a small molecule reduces RMS xenograft growth in mice. Collectively, our study demonstrates that the IRE1α/XBP1 axis is a key regulator of RMS growth and differentiation and highlights that this pathway can be a promising therapeutic target for treatment of patients with RMS.

INTRODUCTION

Rhabdomyosarcoma (RMS) is a highly malignant soft tissue sarcoma that can develop throughout life but occurs more frequently in young children (1-3). RMS is classified into two major subtypes: embryonal rhabdomyosarcoma (ERMS) and alveolar rhabdomyosarcoma (ARMS), each with distinct histological and genetic features. ERMS often arises in the head, neck, or genitourinary tract and commonly harbors genetic alterations such as mutations in the RAS pathway or loss of heterozygosity at chromosome 11p15. Histologically, ERMS resembles immature skeletal muscle cells. ARMS is characterized by a distinctive alveolar growth pattern. ARMS commonly occurs in the extremities, trunk, or head and neck region and is associated with specific chromosomal translocations, such as PAX3-FOXO1 or PAX7-FOXO1, which generate fusion proteins that drive tumor development. For RMS patients with distant metastases, the survival rate is only about 20%-30% (4, 5). RMS exhibits myogenic characteristics, including the expression of myogenic regulatory factors (MRFs) and muscle structural proteins. However, RMS cells fail to exit the cell cycle and undergo terminal differentiation (2, 6, 7). Therefore, agents that inhibit proliferation and promote myogenic differentiation hold promises as novel therapeutics for RMS.

Disruption of proteostasis is a hallmark of nearly all cancer types (8). In mammalian cells, proteostasis is maintained by several stress-responsive signaling pathways, with the unfolded protein response (UPR) of the endoplasmic reticulum (ER) being the most prominent (9). The ER plays a central role in the synthesis, folding, and maturation of approximately one-third of all cellular proteins. Various physiological and pathological conditions can impair protein folding, leading to the accumulation of misfolded or unfolded proteins in the ER lumen, a state referred to as ER stress. During tumor initiation, progression, and metastasis, cancer cells are exposed to numerous intrinsic and extrinsic stressors that induce ER stress. These include the loss of tumor suppressor genes, oncogene activation, oxidative stress, inflammation, hypoxia, lactic acidosis, and nutrient deprivation (e.g., glucose and amino acids) (9, 10). In addition, conventional cancer therapies such as chemotherapy and radiotherapy can further disrupt proteostasis and exacerbate ER stress in tumor cells.

ER stress activates the UPR, which is orchestrated by the cytoplasmic portion of three ER-resident transmembrane sensors, namely inositol-requiring enzyme 1α (IRE1α), protein kinase R-like ER kinase (PERK), and activating transcription factor 6 (ATF6) (9, 11, 12). The primary function of the UPR is to restore ER homeostasis by enhancing protein folding capacity, promoting the degradation of misfolded proteins via ER-associated degradation (ERAD), and modulating protein synthesis and secretion. However, when ER stress persists and exceeds the cell's adaptive capacity, the UPR shifts from a protective role to promoting apoptosis (9, 11, 12). Indeed, available literature suggests that cancer cells activate the UPR to alleviate ER stress caused by excessive protein-folding requirements, mutations, aneuploidy, and metabolically restrictive tumor microenvironment (9, 10). Nevertheless, the specific roles and regulatory mechanisms of the individual UPR branches in different types of cancer remain poorly understood.

The IRE1α is the most evolutionarily conserved ER sensor (13). The cytoplasmic region of IRE1α contains both a serine/threonine kinase and a tandem endoribonuclease (RNase) module. In conditions of ER stress, IRE1α monomers dimerize and undergo autophosphorylation through their kinase domain, leading to allosteric activation of its endoribonuclease domain. The activated RNase cleaves a 26-nucleotide intronic region of X-box protein 1 (XBP1) mRNA, causing a frameshift and translation of its spliced isoform, known as spliced XBP1 (sXBP1). The

sXBP1 protein is an active transcription factor that regulates the gene expression of multiple molecules involved in protein folding and secretion and ERAD pathway (13, 14). Activated IRE1α can also cleave and degrade select mRNAs by a process termed as regulated IRE1α-dependent decay (RIDD), thereby repressing protein synthesis (15, 16). Several recent studies have shown that the IRE1α/XBP1 signaling causes tumorigenesis and progression of several malignancies, such as multiple myeloma (17, 18), chronic lymphocytic leukemia (19), breast cancer (20-22), and colon cancer (23, 24). In addition to its enzymatic activity, IRE1α can also act as a scaffold protein to repress the activation of tumor protein 53 (TP53) through mechanisms potentially involving protein-protein interactions, enabling cell cycle progression in colorectal cancer and multiple myeloma (25).

Recent studies from our group and others have shown that the IRE1α/XBP1 signaling pathway plays a crucial role in skeletal muscle regeneration following both acute and chronic injury (26-28). Additionally, the IRE1α/XBP1 signaling promotes myoblast fusion during myogenic differentiation (29). However, its role and mechanisms of action in RMS remain unknown. In this study, we investigated how IRE1α/XBP1 signaling regulates the proliferation and differentiation of RMS cells. Our findings reveal increased expression of multiple components of the IRE1α/XBP1 pathway in RMS tumor specimens and elevated levels of phosphorylated IRE1α and spliced XBP1 (sXBP1) protein in both ERMS and ARMS cell lines. We further demonstrate that molecular or pharmacological inhibition of IRE1α/XBP1 reduces RMS cell proliferation and improves sensitivity to chemotherapeutic drug vincristine, while promoting their differentiation along the myogenic lineage. In vivo, inducible knockdown of XBP1 significantly impairs tumor growth in RMS xenograft models. Furthermore, our results demonstrate that the IRE1α/XBP1 axis drives RMS progression, at least in part, through upregulating *BMPR1A* expression and enhancing BMP-Smad1 signaling.

RESULTS

Activation of the IRE1α/sXBP1 signaling axis in patient tumor specimens and RMS cell lines. We first analyzed how the gene expression of various components of IRE1α/XBP1 pathway is affected in human RMS samples. Analysis of a publicly available RNA-seq dataset (GSE108022) that includes normal muscle, fusion-positive RMS (FP-RMS) and fusion-negative RMS (FN-RMS) samples showed that the mRNA levels of IRE1α (gene name: *ERN1*) and XBP1 and several downstream molecules including ER chaperons, components of translocon and ERAD, and cell cycle regulators were significantly up-regulated in both FP-RMS and FN-RMS samples compared with normal muscle (**Fig. 1A**). Analysis of another publicly available microarray dataset (GSE141690) that includes 16 normal muscle and 66 RMS samples. Results showed that the mRNA levels of various components of IRE1α/XBP1 axis were significantly upregulated in RMS samples compared to normal muscle (**Fig. 1B**). We also evaluated XBP1 expression levels in different types of sarcoma cell lines using cBioPortal platform. This analysis showed that gene expression of XBP1 is increased across many types of sarcoma cell lines, including RMS (**Fig. 1C**). To further examine the involvement of the IRE1α/XBP1 signaling axis in RMS pathogenesis, we measured the levels of phosphorylated IRE1α (p-IRE1α), total IRE1α, and spliced XBP1 (sXBP1) protein in both ERMS and ARMS cell lines. Primary human myoblasts (HM), ERMS cell lines (RD, HTB82, RH36), and ARMS cell lines (RH30, RH41) were cultured under growth conditions, and protein levels were measured by performing western blot. We observed a marked increase in p-IRE1α, total IRE1α, and sXBP1 protein levels in RD,

HTB82, RH36, and RH41 cells compared to HM. Additionally, there was a modest but statistically significant increase in the levels of p-IRE1α, total IRE1α, and sXBP1 protein in RH30 cells compared to HM (**Fig. 1D-G**). Collectively, these results demonstrate that the IRE1α/XBP1 branch of the UPR is highly activated in human ERMS and ARMS tumor specimens and cell lines.

The IRE1α/XBP1 axis promotes the proliferation of RMS cell lines. To understand the role of IRE1α/XBP1 signaling in RMS, we first generated lentiviral particles expressing a scrambled (SCR), IRE1α, or XBP1 shRNA. Cultured RD cells were transduced with lentiviral particles for 48 h and stable cells were selected by treating with 2μg/ml puromycin for 3 days. The cells were then analyzed by performing western blot for IRE1α and sXBP1 protein. Results showed that the levels of both IRE1α and sXBP1 protein were significantly reduced in RD cells stably expressing IRE1α shRNA whereas the levels of sXBP1 were reduced in RD cultures expressing XBP1 shRNA compared to control cultures expressing SCR shRNA. Interestingly, there was a small but significant increase in the levels of IRE1α protein in XBP1 shRNA-expressing RD cells (**Fig. 2A, B)**. To understand how IRE1α or XBP1 regulates gene expression in RMS cells, we performed bulk RNA sequencing (RNA-Seq) of RD cells expressing SCR, IRE1α, or XBP1 shRNA. Results showed that IRE1α knockdown resulted in the upregulation of 691 genes and downregulation of 3,633 genes, while XBP1 knockdown resulted in the upregulation of 532 genes and downregulation of 1,305 genes compared with controls, with differential expression deemed significant at a p-value threshold of <0.05 (**Fig. S1A, S1B)**. Pathway enrichment analysis using Metascape Annotation tool showed that upregulated genes in IRE1α or XBP1 knockdown RD cells were associated with skeletal system development, muscle structure development, tissue morphogenesis, cytoskeletal in muscle cells, extracellular matrix organization, mitochondria organization, cell adhesion, and regulation of cell differentiation. In contrast, downregulated genes were associated with phosphorylation, EGFR signaling, mitotic cell cycle, cell proliferation, negative regulation of cellular component organization, response to growth factor, and cell division (**Fig. 2C, D**). Heatmap analysis of the DEGs further showed that the mRNA levels of various molecules involved in cell division and proliferation were significantly downregulated in IRE1α or XBP1 knockdown RD cultures compared with control cultures expressing SCR shRNA (**Fig. S1C**).

We next investigated the effect of knockdown of IRE1α or XBP1 on the proliferation of RMS cells using RD (ERMS) and RH41 (ARMS) cell lines as models. The RD and RH41 cells expressing SCR, IRE1α, or XBP1 shRNA were plated at equal number and total number of cells was assessed on day 5. Results showed that knockdown of IRE1α or XBP1 significantly reduced the number of RD or RH41 cells compared to corresponding control cells expressing SCR shRNA (**Fig. 2E**). To further understand the role of the IRE1α/XBP1 pathway in RMS cell proliferation, we also performed an EdU incorporation assay. RD and RH41 cells stably expressing scrambled, IRE1α, or XBP1 shRNA were cultured at equal densities. After 48 h, the cells were labeled with EdU for 2 h, and the proportion of EdU^+ nuclei was detected (**Fig. 2F**). We observed a significant reduction in the proportion of EdU^+ cells in both RD and RH41 cultures expressing IRE1α or XBP1 shRNA compared to corresponding control cells expressing SCR shRNA (**Fig. 2G**). We also measured the effect of knockdown of IRE1α or XBP1 on the proliferation of RH30 cells which express relatively less amounts of IRE1α or XBP1 compared to other RMS cell lines (**Fig. 1D, E**). Interestingly, there was no significant difference in the proliferation of RH30 cells expressing SCR, IRE1α or XBP1 shRNA (**Fig. S1D**).

We also developed Tet-On lentiviral vectors which allow inducible expression of scrambled shRNA or XBP1 shRNA system after treatment with doxycycline (**Fig. 2H**). Using these vectors, we investigated whether inducible knockdown of XBP1 can also reduce the proliferation of RMS cells. Stably expressing Tet-On scrambled shRNA or Tet-on XBP1 shRNA RD cells were plated at equal number in a 96-well plate. After 24h, the cells were treated with 1 µg/ml doxycycline to induce XBP1 knockdown and the number of cells were counted every two days post-doxycycline treatment. Results showed that the number of RD cells expressing Tet-On XBP1 shRNA was significantly reduced compared to control cells transduced with Tet-On scrambled shRNA on day 6 after treatment with doxycycline (**Fig. 2I**).

We next investigated the effect of overexpression of sXBP1 on the proliferation of RMS cells. For this experiment, we engineered a Tet-On lentiviral system that allows inducible expression of sXBP1 upon treatment with doxycycline. RD and RH30 cells stably expressing Tet-On sXBP1 cDNA were plated at equal number. After 24 h, the cultures were treated with 2 µg/ml doxycycline or vehicle alone, and the number of cells was counted at different time points. Results showed that sXBP1 overexpression (OE) led to a small but significant increase in the proliferation of RD cells compared to control cells on day 4 and 6 after treatment with doxycycline (**Fig. 2J**). Intriguingly, overexpression of sXBP1 protein in RH30 cells led to a two-fold increase in cell number after 6 days of treatment with doxycycline (**Fig. 2J**). This differential response between RD and RH30 cells could be attributed to the basal levels of sXBP1 protein. RD cells express higher sXBP1 levels compared to RH30 cells, leading to saturation of endogenous XBP1 in RD cells. Consequently, exogenous sXBP1 overexpression in RD cells does not significantly affect their proliferation. In contrast, the lower endogenous sXBP1 levels in RH30 cells allow for a more pronounced response to exogenous overexpression, resulting in increased cell proliferation. Our western blot analysis confirmed increased expression of sXBP1 in RD and RH30 cells treated with doxycycline (**Fig. 2K**)

To understand the therapeutic potential of inhibition of IRE1α/XBP1 arm of the UPR in RMS, we next investigated whether pharmacological inhibition of IRE1α endonuclease activity using a small molecule 4µ8C (30) also diminishes the proliferation of RMS cells. RD and RH41 cells were treated with vehicle alone or 10 µM 4µ8C for 72 h. Results showed that the number of RD or RH41 cells was significantly reduced in 4µ8C-treated cultures compared to corresponding cultures treated with vehicle alone (**Fig. 2L**). In another experiment, we also assessed cell proliferation by EdU incorporation assay. There was a significant reduction in the proportion of EdU^+ cells in RD and RH41 cultures treated with 4µ8C compared to those treated with vehicle alone (**Fig. 2M, N**). While treatment with 4µ8C reduced the proliferation of RD and RH41 cells, there was no significant effect on the proliferation of human myoblasts (**Fig. S1E**).

Inhibition of IRE1α/XBP1 signaling augments the markers of apoptosis in RMS cell cultures. Prior reports suggest that the activation of UPR protects cancer cells from undergoing apoptosis (8, 10, 19, 21). We next investigated whether the inhibition of IRE1α/XBP1 axis affects the survival of RMS cells. RD and RH41 cells were transduced with lentiviral particles expressing SCR shRNA or XBP1 shRNA. After 5 days, the cells were processed for Annexin V and propidium iodide staining followed by FACS analysis. There was a small but significant increase in the number of Annexin V^+ cells observed in XBP1 shRNA-expressing RD and RH41 cells compared to their controls (**Fig. 3A, B**). We also measured the effect of knockdown of XBP1 on the levels of cleaved PARP and cleaved caspase-3, the two well-established biochemical markers of apoptosis (31). Consistent with Annexin V staining results, we observed

that knockdown of XBP1 increased the levels of cleaved PARP and cleaved caspase-3 in RD and RH41 cells. Silencing of XBP1 also increased the levels of cleaved PARP and cleaved caspase-3 in HTB82 and RH30 cell lines (**Fig. 3C, D**). Moreover, we found that doxycycline-inducible knockdown of XBP1 also increased apoptosis and levels of cleaved PARP in Tet-On XBP1 shRNA-expressing RD cells (Supplemental **Fig. S3**). Finally, pharmacological inhibition of IRE1α/XBP1 axis using 4μ8C augmented the proportion of apoptotic cells and increases the levels of cleaved PARP and cleaved caspase-3 in RD and RH41 cells (**Fig. 3E-H**).

Pharmacological inhibition of IRE1α/XBP1 enhances the cytotoxic effect of vincristine in RMS cells. Prior studies have shown that the activation of UPR can decrease the sensitivity of cancer cells to various chemotherapeutic agents (32). Vincristine is a commonly used chemotherapeutic drug for RMS (33, 34). Therefore, we next investigated whether inhibition of IRE1α/XBP1 could enhance the anti-tumor efficacy of low-dose vincristine (2 nM for RD, RH36, RH30 and 1nM for RH41 cells) in RMS cell lines. RD, RH36, RH30, and RH41 cells were treated with vehicle alone, vincristine, 4μ8C, or a combination of vincristine and 4μ8C. After 5 days, the cells were subjected to Annexin V and PI staining followed by FACS analysis. Results showed that the proportion of apoptotic cells was significantly higher in cultures treated with the combination of vincristine and 4μ8C compared with those treated with either agent alone (**Fig. 4A, B**).

To assess cell viability, we also performed an MTT assay, which measures mitochondrial enzyme activity as an indicator of cellular proliferation and survival. The MTT assay also revealed that combined treatment with vincristine and 4μ8C was significantly more effective in reducing RMS cell viability than treatment with either vincristine or 4μ8C alone (**Fig. 4C**). We also used another approach to study the effect of 4μ8C and vincristine on viability of RMS cells. RD, RH36, RH30, and RH41 cells were plated in 6-well tissue culture plate and treated with vehicle alone, vincristine, 4μ8C, or a combination of vincristine and 4μ8C. After 5 days, dead cells were washed away with PBS, and the live cells remaining attached to the plate were stained with crystal violet. For quantitative estimation, the bound crystal violet dye was solubilized, and the absorbance was measured. Results showed that vincristine and 4μ8C alone reduced cellular viability across all tested cell lines; however, the combination treatment produced a markedly greater effect in reducing the survival of RMS cells (**Fig. 4D, E**).

In a separate experiment, we examined the effect of XBP1 knockdown on vincristine-induced cytotoxicity. RD and RH41 cells were transduced with lentiviral vector expressing either scrambled (SCR) or XBP1 shRNA for 36 h. The cells were then treated with vehicle alone or a low dose of vincristine (i.e., 2 nM) for 5 days, followed by Annexin V staining and FACS analysis. Knockdown of XBP1 significantly increased vincristine-induced apoptosis in both RD and RH41 cells (**Fig. 4F,** Supplemental **Fig. S4**). Collectively, these findings indicate that inhibition of the IRE1α/XBP1 signaling pathway enhances vincristine cytotoxicity and reduces RMS cell survival.

Inhibition of IRE1/XBP1 axis reduces cancer stem cells (CSCs) and epithelial-mesenchymal transition (EMT) phenotype in RD cells. Individual tumors consist of a mixed cell population that differ in function, morphology, and molecular signatures (35-37). Similar to other cancer types, RMS also show heterogeneity in nature, consists of a small subset of CSCs, which may be responsible for tumorigenesis, chemoresistance, and recurrence of the disease (36-42). CSCs of RMS express many stemness-related molecules such as Sox2, Sox9, KLF4, Oct4, and c-Myc

(39, 43). They also express CD133 on their cell surface (40, 41, 43, 44). Our analysis of RNA-Seq dataset showed that mRNA levels of various markers of stemness are significantly reduced in IRE1 or XBP1 knockdown RD cultures compared with control cultures (**Fig. 5A**). Western blot analysis also showed that the protein levels of KLF4 and Sox9 are significantly reduced in XBP1 shRNA expressing RD cells compared to control cells expressing SCR shRNA (**Fig. 5B, C**). By performing FACS analysis, we also evaluated the effect of knockdown of XBP1 on the proportion of CD133-expressing cells. Results showed a significant reduction in the proportion of $CD133^+$ cells in XBP1 knockdown cultures compared with control cultures (**Fig. 5D, E**).

To further elucidate the role of IRE1α/XBP1 signaling in RMS, we turned to a model system in which RMS cells are cultured in stem cell medium in suspension leading to formation of spheres, termed “rhabdospheres". This microenvironment allows only cells with stem-like properties to proliferate and form three-dimensional spheres in suspension culture (41, 43). RD cells stably expressing scrambled or XBP1 shRNA were cultured under non-adherent conditions in serum-free media supplemented with B27, epidermal growth factor (EGF), and basic fibroblast growth factor (bFGF) in a DMEM/F12 base. After 2 weeks of culturing, the images were captured, and diameter of the spheres was measured. Results showed that silencing of XBP1 resulted in significantly smaller spheres compared to corresponding control cells suggesting that IRE1α/XBP1 signaling promotes the self-renewal and proliferation of CSCs in RD cell line (**Fig. 5F, G**).

Our analysis of RNA-Seq dataset also showed that the gene expression of many molecules related to EMT phenotype was significantly downregulated in RD cells following knockdown of IRE1α or XBP1 (**Fig. 5H**). To test whether IRE1α/XBP1 axis has any role in EMT phenotypes, we studied the effect of XBP1 silencing on the invasive and migratory capabilities of RD cells. Interestingly, stable knockdown of XBP1 considerably reduced the migratory capacity of RD cells (**Fig. 5I, J**). Similarly, knockdown of XBP1 led to a marked reduction in the invasive potential of RD cells (**Fig. 5K, L**) suggesting that silencing of XBP1 diminishes the migratory and invasive capacity of RMS cells.

Inhibition of IRE1α/XBP1 signaling augments myogenic differentiation in RMS cells. RMS is a malignant tumor of mesenchymal origin characterized by the proliferation of undifferentiated skeletal muscle cells (2). To determine whether activation of the IRE1α/XBP1 signaling pathway influences RMS cell differentiation, we first analyzed our RNA-seq dataset. Notably, gene expression of numerous molecules involved in muscle differentiation, structural development, and cytoskeleton organization was significantly upregulated in IRE1α- or XBP1-knockdown RD cells compared with control cells (**Fig. 6A**), consistent with the pathway analysis results (**Fig. 2C**). To validate these transcriptomic findings, we examined the effects of IRE1α or XBP1 knockdown on the expression of terminal differentiation markers such as myosin heavy chain (MyHC). The proportion of $MyHC^+$ cells was markedly increased in RD cultures expressing IRE1α or XBP1 shRNA compared with control cultures (**Fig. 6B, C**). Western blot analysis further confirmed elevated MyHC protein levels in IRE1α- and XBP1-depleted RD cells (**Fig. 6D, E**). Similarly, shRNA-mediated knockdown of IRE1α or XBP1 significantly enhanced the expression of MyHC and myogenin in RH41 cells (**Fig. 6F, G**).

To further assess this effect, we employed an inducible XBP1 shRNA system. RD cells transduced with Tet-On XBP1 shRNA lentiviral particles were treated with vehicle or doxycycline, followed by western blot analysis to determine the changes in the levels of MyHC and myogenin protein. Results showed that inducible knockdown of XBP1 led to increased

protein levels of both MyHC and myogenin (**Fig. 6H, I**). We next investigated whether pharmacological inhibition of IRE1α/XBP1 signaling would similarly promote differentiation. Treatment of RD cells with the IRE1α RNase inhibitor 4μ8C significantly increased the proportion of $MyHC^+$ cells compared with controls (**Fig. 6J, K**). Consistent with these findings, western blot analysis showed elevated MyHC and myogenin and reduced sXBP1 protein levels in 4μ8C-treated cultures (**Fig. 6L, M**). Together, these results demonstrate that both molecular and pharmacological inhibition of IRE1α/XBP1 signaling enhances terminal myogenic differentiation in RMS cells.

IRE1α/XBP1 signaling regulates BMPR1A expression in RMS cells. To elucidate the mechanisms by which IRE1α/XBP1 signaling promotes proliferation and suppresses differentiation in RMS cells, we analyzed our RNA-seq dataset. Notably, knockdown of IRE1α or XBP1 markedly reduced the expression of several components of the BMP signaling pathway, including *BMPR1A* (**Fig. 7A**). Analysis of a publicly available gene expression dataset (GSE108022) further revealed that *BMPR1A* transcript levels were significantly elevated in both fusion-positive (FP-RMS) and fusion-negative (FN-RMS) tumors compared with normal skeletal muscle (**Fig. 7B**). Previous studies indicate that BMP signaling can exert context-dependent effects, functioning as either a tumor suppressor or promoter depending on cancer type (45). However, its role in RMS remains unclear. To investigate whether BMP signaling is aberrantly activated in RMS, we compared the protein levels of BMPR1A, phosphorylated Smad1 (p-Smad1), and total Smad1 between RD cells and normal human myoblasts (HM). We observed a marked increase in BMPR1A, p-Smad1, and total Smad1 protein levels in RD cells relative to HM (**Fig. 7C, D**). To explore the link between IRE1α/XBP1 signaling and BMPR1A expression, we next examined the effect of XBP1 knockdown on BMP pathway components in RD cells. Knockdown of XBP1 significantly decreased BMPR1A and p-Smad1 protein levels without affecting total Smad1 (**Fig. 7E, F**). Similarly, pharmacological inhibition of IRE1α RNase activity using 4μ8C reduced BMPR1A and p-Smad1 levels (**Fig. 7G, H**). Conversely, overexpression of the spliced, active form sXBP1 increased BMPR1A and p-Smad1 protein levels in both RD and RH30 cells (**Fig. 7I, J**). Given that sXBP1 functions as a transcription factor, we hypothesized that it may directly regulate *BMPR1A* transcription by binding to its regulatory region. Genome analysis using the UCSC Genome Browser identified a putative sXBP1-binding site within the enhancer region of the *BMPR1A* gene (**Fig. 7K**). To validate this prediction, we performed chromatin immunoprecipitation (ChIP) assays followed by semi-quantitative and quantitative PCR (qPCR) using primers spanning the predicted binding regions (100-200bp). ChIP results demonstrated significant enrichment of sXBP1 at the *BMPR1A* enhancer region in RD cells. The ChIP experiment was validated by performing semi-quantitative PCR for positive control *RPL30* using Histone H3 antibody (**Fig. 7L**). Quantitative analysis by qPCR further showed a ~15-fold increase in sXBP1 binding to the *BMPR1A* enhancer compared to IgG control (**Fig. 7M**). Collectively, these findings indicate that sXBP1 directly binds to and transcriptionally regulates *BMPR1A* expression, thereby modulating BMP signaling activity in RMS cells.

Inhibition of BMPR1A-mediated signaling reduces proliferation and promotes differentiation in RMS cells. Since the role of BMPR1A-mediated signaling in RMS remains unclear, we next generated lentiviral particles expressing BMPR1A shRNA to assess the effects of BMPR1A depletion on RMS cell proliferation and differentiation. RD cells were transduced

with scrambled or BMPR1A shRNA for 72 h, followed by EdU incorporation assays. Results showed that knockdown of BMPR1A markedly reduced the proportion of EdU^+ nuclei in RD cells, indicating a suppression of cell proliferation (**Fig. 8A, B**). Furthermore, BMPR1A knockdown significantly increased the expression of myogenic differentiation markers, including myogenin and MyHC, compared with control cultures (**Fig. 8C, D**). LDN193189 is a small molecule chemical compound that acts as a potent and selective inhibitor of BMP signaling which functions through inhibiting BMP type I receptors (46). To pharmacologically inhibit BMP signaling, RD cells were treated with vehicle alone or LDN193189 (0.1 μM) for 72 h followed by immunostaining for myogenin or MyHC protein. Interestingly, treatment with LDN193189 drastically increased the number of $myogenin^+$ cells in RD cultures (**Fig. 8E, F**). Furthermore, treatment with LDN193189 increased the number of $MyHC^+$ cells and differentiation index in RD cell cultures (**Fig. 8G, H**). Western blot analysis also showed that the levels of myogenin and MyHC protein are increased in LDN193189-treated RD cells compared to control cells (**Fig. 8 I, J**). Collectively, these results indicate that BMPR1A-mediated signaling supports RMS cell proliferation while restraining their terminal differentiation into skeletal muscle.

Inducible knockdown of XBP1 suppresses growth of RD xenografts in nude mice. To determine the role of XBP1 in RMS tumor growth in vivo, we examined the effect of XBP1 silencing on subcutaneous RD xenografts in nude mice. RD cells were stably transduced with Tet-On XBP1 shRNA and firefly luciferase lentiviral particles and subsequently injected subcutaneously into the right flank of male nude mice. When the tumor size reached ~ 150 mm^3, the mice were randomized into two groups: one receiving doxycycline-containing chow and the other receiving standard chow. Body weight and tumor volume were monitored weekly by caliper measurements. No significant differences in body weight were observed between the two groups throughout the study (**Fig. 9A**). Notably, within two weeks of doxycycline administration, tumor volumes in the doxycycline-treated group were significantly reduced compared with controls, and this difference continued to increase through day 28 (**Fig. 9B**). In vivo bioluminescence imaging following luciferin injection confirmed markedly smaller tumors in doxycycline-treated mice after 25 days (**Fig. 9C**). At the end of the study, tumors were excised and weighed. Tumor wet weight in the doxycycline-treated group was reduced by approximately 50% relative to controls (**Fig. 9D, E**). To exclude potential effects of doxycycline alone, a parallel experiment was performed using RD cells expressing Tet-On scrambled shRNA and luciferase. No significant differences in body weight, tumor volume, or tumor wet weight were observed between doxycycline-treated and control mice in this cohort (**Fig. S3**), indicating that doxycycline treatment per se does not affect RD tumor growth.

We next performed histological and biochemical analyses of tumor samples. Hematoxylin and eosin (H&E) staining of tumor sections revealed reduced tumor cell density and the presence of multinucleated cells in XBP1 knockdown tumors, suggestive of growth arrest and myogenic differentiation (**Fig. 9F**). Immunostaining for Ki67, a proliferation marker, demonstrated a marked reduction in $Ki67^+$ cells in doxycycline-treated tumors (**Fig. 9G, H**). Conversely, there was a significant increase in $myogenin^+$ cells, indicating enhanced myogenic differentiation (**Fig. 9I, J**). Western blot analysis confirmed efficient XBP1 knockdown, as evidenced by a substantial reduction in sXBP1 protein levels in tumors of doxycycline-treated mice. Additionally, BMPR1A and phosphorylated Smad1 (p-Smad1) protein levels were also significantly reduced in tumors of doxycycline-treated mice compared with controls (**Fig. 9K,**

L). To complement these molecular findings, we also evaluated the effect of pharmacological inhibition of IRE1α/XBP1 signaling on RD xenograft growth. Nude mice bearing subcutaneous RD tumors (~150 mm^3) were treated with vehicle or the IRE1α RNase inhibitor 4μ8C (10 mg/kg) twice per week by intraperitoneal (IP) injection for 4 weeks. After 4 weeks of treatment, the final dose of 4μ8C was administered 12 h before euthanizing the mice. Treatment with 4μ8C significantly reduced RD tumor size in mice compared with vehicle controls (**Fig. 9M, N**). Together, these results demonstrate that both molecular and pharmacological inhibition of the IRE1α/XBP1 axis markedly suppresses RMS tumor growth in vivo.

DISCUSSION

Despite significant therapeutic advances, the prognosis for children with aggressive or metastatic RMS) remains poor, largely because the molecular mechanisms driving tumorigenesis and chemoresistance are not fully understood (4, 7, 34, 47). Accumulating evidence indicates that the IRE1α/XBP1 branch of the UPR exerts context-dependent effects in cancer, generally promoting tumor growth and therapeutic resistance through adaptation to ER stress, yet functioning as a tumor suppressor under specific conditions (22, 48-50). However, the role and mechanisms by which IRE1α/XBP1 signaling axis regulates RMS pathogenesis remains poorly understood.

Through integrated analyses of patient-derived tumor datasets, RMS cell lines, and xenograft models, we demonstrate that the IRE1α/XBP1 axis is constitutively activated in RMS subtypes. These findings are consistent with reports of persistent IRE1α/XBP1 activation in other malignancies, including breast, prostate, and pancreatic cancers, sarcomas, and glioblastoma (51-54). We further show that genetic or pharmacological inhibition of IRE1α/XBP1 signaling suppresses RMS cell proliferation and survival, promotes terminal myogenic differentiation, and enhances sensitivity to chemotherapeutic agents, such as vincristine. Finally, our experiments demonstrate that the sXBP1 directly regulates *BMPR1A* transcription, thereby linking UPR activation to BMP-Smad signaling and the maintenance of an undifferentiated, stem-like phenotype in RMS.

Our findings suggest that the activation of IRE1α/XBP1 signaling in RMS is a survival mechanism that supports the high biosynthetic demands of rapidly proliferating tumor cells. Silencing of IRE1α or XBP1 reduced proliferation of both ERMS and ARMS cell lines whereas forced expression of sXBP1 augmented the proliferation of RH30 cells. RNA-Seq analysis following knockdown of IRE1α or XBP1 also revealed downregulation of many cell cycle-related genes, particularly those involved in mitotic progression and growth factor signaling, suggesting that this pathway promotes RMS cell proliferation at the transcriptional level (**Fig. 2**). Interestingly, gene expression of many molecules involved in muscle structure development and differentiation was upregulated, suggesting that the inhibition of IRE1α/XBP1 axis mitigates the impaired differentiation in RMS (**Fig. 6**). Consistent with these transcriptional changes, our results demonstrated that pharmacologic inhibition of IRE1α RNase activity with 4μ8C reduced proliferation and survival and improved terminal differentiation in RMS cells.

While inhibition of IRE1α/XBP1 signaling alone modestly induced apoptosis, combined treatment with the IRE1α inhibitor 4μ8C and vincristine produced markedly synergistic cytotoxic effects. This treatment enhanced apoptotic cell death, reduced metabolic activity, and suppressed colony formation across multiple RMS cell lines (**Fig. 4**). These results are consistent with prior studies demonstrating that activation of the UPR can protect cancer cells from chemotherapeutic stress by attenuating ER stress-induced apoptosis (32). Previously it was reported that constitutive IRE1α RNase activity promotes the production of pro-tumorigenic

factors and confers chemoresistance to paclitaxel in triple-negative breast cancer. Inhibition of IRE1α RNase activity enhances paclitaxel-induced tumor regression and delays post-therapy tumor relapse (55). Similarly, activation of IRE1α/XBP1 pathway has been found to promote resistance to cytotoxic chemotherapy in lung cancer primarily through increasing the gene expression of multidrug resistance protein 1, which facilitates drug extrusion (56). Although molecular underpinning was unknown, a prior study has also reported that pharmacological inhibition of the components of the UPR reduces the survival of cultured RMS cells (54). In agreement to these published reports, our findings in the present study also revealed that RMS cells are selectively dependent on the IRE1α/XBP1 signaling for their proliferation and survival, highlighting this pathway as a promising therapeutic target.

Recent studies have also suggested the role of UPR in the maintenance of stemness in various malignancies, including glioblastoma, breast cancer, and hepatocellular carcinoma, where XBP1 activation enhances self-renewal and chemoresistance (51-53). Our RNA-Seq analysis and immunoblotting revealed that knockdown of either IRE1 or its downstream effector XBP1 in RD cells resulted in a marked decrease in the expression of multiple stemness markers suggesting that the IRE1α/XBP1 signaling axis plays a critical role in maintaining the CSC-like phenotype in RMS (**Fig. 5**). While the exact mechanisms remain unknown, sXBP1 may directly augment the gene expression of various cancer stemness-related molecules. In addition, sXBP1 can directly or indirectly regulate gene expression of molecules involved in protein folding, redox balance, and lipid biosynthesis, which support the metabolic flexibility of CSCs. IRE1α signaling may also interact with other oncogenic pathways, such as PI3K/AKT, Wnt/β-catenin, or Notch (49, 57), thereby reinforcing the stemness network and promoting RMS cell survival under stress. In addition to its role in CSC maintenance, IRE1α/XBP1 signaling appears to regulate EMT in RMS. Our RNA-seq analysis revealed downregulation of many EMT-associated genes following knockdown of IRE1α or XBP1, and transwell assays confirmed that XBP1 silencing reduced both migratory and invasive capacities of RD cells (**Fig. 5**). Collectively, these results suggest that IRE1α/XBP1 signaling increases RMS stemness and EMT phenotypes, processes that are often interlinked and contribute to tumor aggressiveness.

One of the prominent features of RMS is failure of myogenic differentiation (2, 6, 58). The results of the present study demonstrate that inhibition of IRE1α/XBP1 signaling upregulates the gene expression of differentiation markers, such as myogenin and MyHC in both ERMS and ARMS cells (**Fig. 6**). The upregulation of myogenic genes upon pathway inhibition indicates that IRE1α/XBP1 actively represses terminal differentiation, possibly through transcriptional regulation of differentiation-inhibitory pathways. During myogenesis, the BMPR1A signaling plays a crucial role in coordinating muscle progenitor proliferation and differentiation. Specifically, activation of BMPR1A-mediated signaling prevents premature differentiation, allowing for expansion of the muscle progenitor cells before promoting their fusion to form multinucleated myotubes (59, 60). However, constitutive activation of BMP signaling can keep the progenitor cells in proliferative state which can lead to development of cancer. Indeed, previous studies have demonstrated that the activation of BMPR1A-Smad1 signaling promotes the stemness and proliferation of cancer cells (45, 61, 62). Our experiments revealed that RMS cells expressed higher BMPR1A and p-Smad1 levels than normal human myoblasts, and both molecular and pharmacological inhibition of XBP1 decreased BMPR1A and p-Smad1 expression. Conversely, overexpression of sXBP1 protein upregulated BMPR1A and activated downstream Smad1 signaling. The ChIP-qPCR assay also confirmed direct binding of sXBP1 to the *BMPR1A* enhancer, establishing a transcriptional link between UPR activation and

BMP signaling (**Fig. 7**). Finally, our results demonstrated that knockdown or pharmacological inhibition of BMPR1A-mediated signaling mimicked the effects observed by XBP1 inhibition, resulting in reduced proliferation and enhanced myogenic differentiation (**Fig. 8**). Altogether, these results suggest a novel IRE1α-XBP1-BMPR1A regulatory axis that integrates UPR signaling with pathways governing cell fate decisions in RMS.

Our experiments also showed that inducible knockdown of XBP1 markedly suppresses the growth of RD xenografts in nude mice, establishing a crucial role for XBP1 in promoting RMS tumor progression in vivo. Using a doxycycline-inducible shRNA system, we showed that suppression of XBP1 expression leads to a substantial reduction in tumor volume and weight. Consistent with the genetic approach, pharmacological inhibition of IRE1α RNase activity using 4μ8C produced comparable tumor-suppressive effects, further validating the functional importance of the IRE1α/XBP1 signaling axis in RMS growth. Mechanistically, reduced BMPR1A and p-Smad1 levels in XBP1-deficient tumors suggest that XBP1 sustains RMS growth, at least in part, through BMP/Smad signaling. The reduction in tumor burden in mice following XBP1 knockdown was accompanied by reduced proliferation and enhanced differentiation of RD cells evidenced by a pronounced reduction in $Ki67^+$ cells and a concomitant increase in $myogenin^+$ cells. These findings suggest that XBP1 silencing not only impedes tumor cell growth but also promotes myogenic differentiation (**Fig. 9**) which is consistent with our in vitro findings showing that inhibition of the IRE1α/XBP1 signaling can relieve differentiation blocks in RMS cells (**Fig. 6**). The presence of multinucleated cells in XBP1-deficient tumors further supports the notion that suppression of XBP1 reactivates differentiation programs that are normally impaired in RMS.

In summary, our study provides initial evidence that the IRE1α/XBP1 signaling axis is a central regulator of RMS growth. Since this pathway intersects multiple oncogenic processes, including proliferation, survival, stemness, and differentiation blockade, its inhibition represents a multifaceted approach to RMS therapy.

METHODS

Cell culture. RD, RH30, and HTB82 rhabdomyosarcoma cell lines were obtained from the American Type Culture Collection (ATCC). RH36 and RH41 cell lines were kindly provided by the Houghton laboratory (UT Health San Antonio, Texas). RD and RH36 cells were maintained in Dulbecco's modified Eagle medium (DMEM) supplemented with 10% fetal bovine serum (FBS) and 1% penicillin-streptomycin (P/S). RH30 and RH41 cells were cultured in RPMI 1640 medium supplemented with 10% FBS and 1% P/S. HTB82 cells were cultured in McCoy's 5A medium supplemented with 10% FBS and 1% P/S. Human skeletal muscle myoblasts were purchased from ThermoFisher Scientific and maintained in Iscove's Modified Dulbecco's Medium (IMDM) supplemented with 20% FBS, 10% horse serum, and 20 ng/mL basic fibroblast growth factor. All cell lines were routinely tested and confirmed to be mycoplasma-free by using Universal Mycoplasma Detection Kit (ATCC 30-1012K, ATCC, USA).

Generation of plasmid constructs. The target siRNA sequence for human IRE1α, XBP1, or BMPR1A mRNA was identified using BLOCK-iT™ RNAi Designer online software (Life Technologies). The shRNA oligonucleotides were synthesized to contain the sense strand of target sequences for human IRE1α (5'- GGT GGA ATG CCA CCT ACT TTG-3'), human XBP1 (5'-GGA ATG ATC CAA TAC TGT TGC-3'), or human BMPR1A (5'-GGA GAA ACC ACA TTA GCT TCA-3'), short spacer (CTCGAG), and the reverse complement sequences followed

by five thymidines as an RNA polymerase III transcriptional stop signal. Oligonucleotides were annealed and cloned into pLKO.1-mCherry-Puro with AgeI/EcoRI sites. For inducible knockdown, the XBP1 shRNA sequence was inserted into the pLKO-Tet-On plasmid (Addgene plasmid #21915). For Tet-On–inducible overexpression of sXBP1, the coding sequence of sXBP1 was subcloned from pCMV5-Flag-XBP1s (Addgene plasmid #63680) into the pLKO-Tet-On backbone.

Lentivirus production, transduction, and stable expression. Lentiviral particles were generated following a protocol as described (29). Briefly, pLKO.1 or pLKO–Tet-On plasmids encoding scrambled, IRE1α, XBP1, or BMPR1A shRNA, or sXBP1, were co-transfected with packaging plasmids psPAX2 and pMD2.G into HEK293T cells using polyethylenimine (PEI; 1 µg/mL). After 48 h, culture supernatants were collected, centrifuged at 4,500 rpm for 15 min to remove cell debris, and filtered through a 0.45-µm membrane. RMS cells were transduced with viral supernatants by centrifugation in the presence of 6 to 10 µg/ml polybrene (Sigma-Aldrich). After 24 h, the medium was replaced with fresh growth medium. To establish stable cell lines, transduced cells were selected with 2 µg/mL puromycin for 2-3 passages beginning 72 h post-transduction. For inducible knockdown or overexpression, Tet-On RMS cells were treated with 1 µg/ml doxycycline for 3-5 days prior to experiments.

Cell proliferation assay. RMS cell proliferation was evaluated as previously described (63). Cells were seeded at 1,000 cells per well in PhenoPlate™ 96-well tissue culture plates (Revvity, USA). Plates were scanned using the EnSight Multimode Plate Reader with well-imaging technology (PerkinElmer, MA), and cell counts were obtained through digital phase and bright-field imaging. To evaluate pharmacological effects, cells were treated with chemical compounds after overnight seeding, followed by regular scanning and cell counting. For experiments using the Tet-On system, cells were treated with doxycycline (1 µg/ml) after overnight seeding, with subsequent imaging and counting performed at regular intervals.

EdU incorporation assay. DNA synthesis was assessed using the Click-iT™ Plus EdU Alexa Fluor™ 488 Imaging Kit (Invitrogen, USA). RMS cells were incubated with 1 µg/mL EdU for 2 h, fixed with 4% paraformaldehyde, and permeabilized with 0.5% Triton X-100. EdU incorporation was visualized using the Click-iT reaction with Alexa Fluor™ 488 dye, and nuclei were counterstained with DAPI. Images were acquired using a fluorescence microscope, and the percentage of EdU□ nuclei relative to total DAPI□ nuclei was quantified using NIH ImageJ software. Three to four images from each biological replicate were analyzed.

Cell viability assay. Approximately 5×10^3 cells were seeded in 6-well plates containing 2 ml of culture medium per well and maintained for 5 days with medium change after 48 h. Dead cells were removed by washing the wells with PBS. The adherent cells were fixed and stained with 0.25% crystal violet dye in 20% methanol and images were captured. For quantification, the bound dye was solubilized in 1 ml of 10% acetic acid per well, incubated for 15 min at room temperature with gentle shaking, diluted 1:4 with water, and absorbance was measured at 590 nm using a SpectraMax® i3x microplate reader (Molecular Devices).

Sphere formation assay. Approximately 1×10^3 RD cells stably transduced with scrambled or XBP1 shRNA were seeded per well in 24-well low-attachment Nunclon™ Sphera™ dishes

(Thermo Fisher Scientific, USA). Each well contained 1 ml of DMEM/F12 medium supplemented with B27, epidermal growth factor (EGF, 10 ng/mL), and basic fibroblast growth factor (bFGF, 10 ng/mL). After 14 days of incubation, the images of the spheres were acquired using a microscope and the diameter of the sphere was measured.

Immunofluorescence. RMS cells stably expressing scrambled (SCR), IRE1α, or XBP1 shRNA were cultured for 5 days. The cultures were washed with PBS, fixed with 4% paraformaldehyde (PFA) for 15 min at room temperature, and permeabilized with 0.5% Triton X-100 in PBS for 15 min. Cells were then blocked with 5% goat serum in PBS containing 0.1% Triton X-100. The anti-MyHC (clone MF20) primary antibody was diluted 1:50 in 5% goat serum and incubated with the cells overnight at 4°C. After washing with PBST, cells were incubated with goat anti-mouse secondary antibody (diluted 1:300 in 5% goat serum) for 1 h at room temperature. Nuclei were counterstained with DAPI for 15 min. Images were acquired using a fluorescence inverted microscope (Nikon Eclipse TE2000-U) equipped with a digital camera (Digital Sight DS-Fi1). The percentage of MyHC□ cells was quantified using ImageJ software.

Differentiation index. Differentiation of RMS cells was quantified by measuring the differentiation index which is defined as: (Number of nuclei in $MyHC^+$ cells/Total number of nuclei) × 100.

Transwell migration and invasion assay. Transwell assays were performed using Boyden chambers (Corning Inc., Corning, NY, USA). For migration assays, 5×10^4 RD or RH30 cells in 200 μl serum-free DMEM were seeded into the upper chamber, while 800 μl of DMEM containing 10% FBS was added to the lower chamber as a chemoattractant. After 24 h incubation, cells that migrated through the membrane were fixed and stained with 0.1% crystal violet. For invasion assays, the procedure was identical except that the upper surface of the membrane was pre-coated with 100 μL of 300 μg/mL Matrigel (BD Biosciences, San Jose, CA, USA). Images of crystal violet-stained cells on the lower membrane surface were captured, and signal intensity normalized to total area was quantified using ImageJ software (NIH).

Annexin V staining and FACS analysis. Cell viability and apoptosis were assessed by Annexin V-FITC and propidium iodide (PI) staining using the Annexin V-FITC Apoptosis Detection Kit, according to the manufacturer's instructions (Abcam). Stained cells were analyzed by flow cytometry.

MTT assay. Cell growth and viability of control and IRE1α- or XBP1-knockdown RMS cells were evaluated using the MTT assay. Briefly, RMS cells stably expressing scrambled, IRE1α, or XBP1 shRNA were seeded at 5×10^3 cells per well in a 96-well plate and cultured for 3 days. Cells were then incubated with MTT solution (0.5 mg/mL) for 4 h at 37°C. The medium was removed, and 100 μl of DMSO was added to each well to dissolve the formazan crystals. Absorbance was measured at 570 nm using a SpectraMax® i3x microplate reader (Molecular Devices). Cell viability was expressed as the percentage relative to corresponding control cells.

Western Blot. Cultured RMS cell lines or RD tumor samples were washed with PBS and homogenized in lysis buffer A (50□mM Tris-Cl [pH 8.0], 200□mM NaCl, 50□mM NaF, 1□mM dithiothreitol, 1□mM sodium orthovanadate, 0.3% IGEPAL, and protease inhibitors).

Approximately, 40 μg protein was resolved on each lane on 8-10% SDS-PAGE gel, transferred onto a PVDF membrane, and probed using a specific primary antibody described in supplemental **Table S1**. Bound antibodies were detected by secondary antibodies conjugated to horseradish peroxidase (Cell Signaling Technology). Signal detection was performed by an enhanced chemiluminescence detection reagent (Bio-Rad). Approximate molecular masses were determined by comparison with the migration of prestained protein standards (Bio-Rad). Uncropped gel images are presented in **Fig. S5**.

Chromatin immunoprecipitation (ChIP) assay. ChIP was performed using SimpleChIP enzymatic Chromatin IP kit (Cell Signaling Technology, Cat #9003) according to the manufacturer's suggested protocol. Briefly, 6 x 10^6 RD cells maintained under growth condition were crosslinked followed by purification of nuclei, and chromatin shearing by sonication (eight times, 20 s each). Sheared chromatin was incubated overnight with antibodies against sXBP1 (Cell Signaling Technology) or Histone H3 (Cell Signaling Technology) followed by incubation with Protein G magnetic beads. Normal Rabbit IgG (Cell Signaling Technology) was used as a negative control for the immunoprecipitation experiment. Magnetic beads were briefly washed, and chromatin DNA was eluted, reverse crosslinked, and purified. Purified DNA was analyzed for enrichment of 100-150 bp sequences by quantitative real time-PCR (40 cycles) or semi-quantitative standard PCR using primer set (Forward: AGC GGT TAA CAA ACT GTT CAG A, Reverse: CCA GAA TAC GAT GTT CCT GGG T) designed for binding sites in the BMPR1A enhancer region. The fold change between negative control IgG and anti-sXBP1 groups was calculated using $2^{-\Delta\Delta Ct}$ formula normalized by signal from 2% input.

RNA-sequencing and data analyses. Total RNA from control, IRE1α, or XBP1 knockdown RD cells was extracted using TRIzol reagent (Thermo Fisher Scientific) using RNeasy Mini Kit (QIAGEN) according to the manufacturers' protocols. The mRNA-seq library was prepared using poly (A)-tailed enriched mRNA at the UT Cancer Genomics Center using the KAPA mRNA HyperPrep Kit protocol (KK8581, Roche, Holding AG, Switzerland) and KAPA Unique Dual-indexed Adapter kit (KK8727, Roche). The Illumina NextSeq550 was used to produce 75 base paired-end mRNA-seq data at an average read depth of ~38 M reads/sample. RNA-seq fastq data were processed using CLC Genomics Workbench 20 (Qiagen). Illumina sequencing adapters were trimmed, and reads were aligned to the mouse reference genome Homo Sapiens (GRCh38/hg38). Normalization of RNA-seq data were performed using a trimmed mean of M values. Genes with $|Log_2FC| \geq 0.25$ and p-value < 0.05 were assigned as differentially expressed genes (DEGs) and represented in volcano plot using ggplot function in R software (v 4.2.2). Pathway enrichment analysis associated with the up-regulated and down-regulated genes were identified using the Metascape gene annotation and analysis tool (metascape.org) as described (64, 65). Heatmaps were generated using the heatmap.2 function (66) using z-scores calculated based on transcripts per million (FPKM) values. TPM values were converted to log (FPKM+1) to handle zero values. Genes involved in specific pathways were manually selected for heatmap expression plots. The average absolute TPM values for the control group are provided in **Table S2**.

Xenograft growth mouse model. Six-week-old male Nu/Nu mice were purchased from Charles River Laboratories. RD cells expressing Tet-On SCR or XBP1 shRNA along with luciferase were suspended in Matrigel (Corning) and approximately 5×10^6 cells in 50% Matrigel (Sigma-

Aldrich) were injected subcutaneously into the flank of each mouse. Body weight and tumor growth was monitored weekly, and tumor length (L) and width (W) were measured. Tumor volume was calculated using the formula 0.5 × L × W^2. Tumor growth was further assessed by bioluminescence imaging using a Xenogen IVIS® system (PerkinElmer). When tumor volumes reached approximately 50-100 mm^3, mice were randomly assigned to 2 groups. One group received standard chow (control), and the other group received doxycycline-containing chow. Mice were euthanized after 4 weeks of doxycycline treatment. For pharmacological studies, approximately 5×10^6 RD cells suspended in 50% Matrigel were injected subcutaneously into the flank of each mouse. When the tumor volume reached approximately 50-100 mm^3, mice received intraperitoneal injections of 4μ8C (10 mg/kg; diluted in 5% DMSO and 95% corn oil) or vehicle (control) every other day. Mice were euthanized after 4 weeks of vehicle or 4μ8C treatment. The animal protocol was approved by the Institutional Animal Care and Use Committee (IACUC) of the University of Houston.

Histology and Immunohistochemistry. Tumors were isolated and processed for histological and biochemical analyses. Tumor samples were fixed in 4% paraformaldehyde overnight at 4°C, washed with cold PBS, and embedded in Frozen Section Compound (FSC22, Leica, USA). Cryosections of 10 µm thickness were prepared and stained with hematoxylin and eosin (H&E). Sections were also immunostained for Ki67 and myogenin protein. Nuclei were counterstained by DAPI.

Statistical analysis. Results are expressed as means ± SD. An unpaired, 2-tailed Student's *t* test was used to compare quantitative data populations with normal distribution and equal variance. The value of $p < 0.05$ was considered significant.

Acknowledgements. We are grateful to Dr. Peter J Houghton of The University of Texas Health Science Center at San Antonio, Texas for providing RH36 and RH41 cell lines. We are also grateful to Dr. Darabi of University of Houston for providing HM cells. We thank technical support from the Cancer Prevention and Research Institute of Texas (CPRIT RP180734) core for RNA-seq experiments.

Data availability. All other raw data generated for this study has been included with this manuscript.

Authors' contributions. AK, BG, and MVT designed the work. ATV, ASJ, PTH, and MTS performed the experiments and analyzed the results. ATV, ASJ, and AK wrote the manuscript. All authors edited and finalized the manuscript.

References

1. Hawkins, D. S., Spunt, S. L., Skapek, S. X., and Committee, C. O. G. S. T. S. (2013) Children's Oncology Group's 2013 blueprint for research: Soft tissue sarcomas. *Pediatr Blood Cancer* **60**, 1001-1008

2. Kashi, V. P., Hatley, M. E., and Galindo, R. L. (2015) Probing for a deeper understanding of rhabdomyosarcoma: insights from complementary model systems. *Nat Rev Cancer* **15**, 426-439

3. Ciarapica, R., Carcarino, E., Adesso, L., De Salvo, M., Bracaglia, G., Leoncini, P. P., Dall'agnese, A., Verginelli, F., Milano, G. M., Boldrini, R., Inserra, A., Stifani, S., Screpanti, I., Marquez, V. E., Valente, S., Mai, A., Puri, P. L., Locatelli, F., Palacios, D., and Rota, R. (2014) Pharmacological inhibition of EZH2 as a promising differentiation therapy in embryonal RMS. *BMC Cancer* **14**, 139

4. Malempati, S., and Hawkins, D. S. (2012) Rhabdomyosarcoma: review of the Children's Oncology Group (COG) Soft-Tissue Sarcoma Committee experience and rationale for current COG studies. *Pediatr Blood Cancer* **59**, 5-10

5. Xia, S. J., Pressey, J. G., and Barr, F. G. (2002) Molecular pathogenesis of rhabdomyosarcoma. *Cancer Biol Ther* **1**, 97-104

6. Keller, C., and Guttridge, D. C. (2013) Mechanisms of impaired differentiation in rhabdomyosarcoma. *FEBS J* **280**, 4323-4334

7. Pal, A., Chiu, H. Y., and Taneja, R. (2019) Genetics, epigenetics and redox homeostasis in rhabdomyosarcoma: Emerging targets and therapeutics. *Redox Biol* **25**, 101124

8. Lv, X., Lu, X., Cao, J., Luo, Q., Ding, Y., Peng, F., Pataer, A., Lu, D., Han, D., Malmberg, E., Chan, D. W., Wang, X., Savage, S. R., Mao, S., Yu, J., Peng, F., Yan, L., Meng, H., Maneix, L., Han, Y., Chen, Y., Yao, W., Chang, E. C., Catic, A., Lin, X., Miles, G., Huang, P., Sun, Z., Burt, B., Wang, H., Wang, J., Yao, Q. C., Zhang, B., Roth, J. A., O'Malley, B. W., Ellis, M. J., Rimawi, M. F., Ying, H., and Chen, X. (2023) Modulation of the proteostasis network promotes tumor resistance to oncogenic KRAS inhibitors. *Science* **381**, eabn4180

9. Wang, M., and Kaufman, R. J. (2014) The impact of the endoplasmic reticulum protein-folding environment on cancer development. *Nat Rev Cancer* **14**, 581-597

10. Chevet, E., Hetz, C., and Samali, A. (2015) Endoplasmic reticulum stress-activated cell reprogramming in oncogenesis. *Cancer Discov* **5**, 586-597

11. Wu, J., and Kaufman, R. J. (2006) From acute ER stress to physiological roles of the Unfolded Protein Response. *Cell Death Differ* **13**, 374-384

12. Hetz, C. (2012) The unfolded protein response: controlling cell fate decisions under ER stress and beyond. *Nat Rev Mol Cell Biol* **13**, 89-102

13. Le Goupil, S., Laprade, H., Aubry, M., and Chevet, E. (2024) Exploring the IRE1 interactome: From canonical signaling functions to unexpected roles. *J Biol Chem* **300**, 107169

14. Park, S. M., Kang, T. I., and So, J. S. (2021) Roles of XBP1s in Transcriptional Regulation of Target Genes. *Biomedicines* **9**, 791

15. Maurel, M., Chevet, E., Tavernier, J., and Gerlo, S. (2014) Getting RIDD of RNA: IRE1 in cell fate regulation. *Trends Biochem Sci* **39**, 245-254

16. Hollien, J., Lin, J. H., Li, H., Stevens, N., Walter, P., and Weissman, J. S. (2009) Regulated Ire1-dependent decay of messenger RNAs in mammalian cells. *J Cell Biol* **186**, 323-331

17. Harnoss, J. M., Le Thomas, A., Shemorry, A., Marsters, S. A., Lawrence, D. A., Lu, M., Chen, Y. A., Qing, J., Totpal, K., Kan, D., Segal, E., Merchant, M., Reichelt, M., Ackerly Wallweber, H., Wang, W., Clark, K., Kaufman, S., Beresini, M. H., Laing, S. T., Sandoval, W., Lorenzo, M., Wu, J., Ly, J., De Bruyn, T., Heidersbach, A., Haley, B., Gogineni, A., Weimer, R. M., Lee, D., Braun, M. G., Rudolph, J., VanWyngarden, M. J., Sherbenou, D. W., Gomez-Bougie, P., Amiot, M., Acosta-Alvear, D., Walter, P., and Ashkenazi, A. (2019) Disruption of IRE1alpha through its kinase domain attenuates multiple myeloma. *Proc Natl Acad Sci U S A* **116**, 16420-16429

18. Carrasco, D. R., Sukhdeo, K., Protopopova, M., Sinha, R., Enos, M., Carrasco, D. E., Zheng, M., Mani, M., Henderson, J., Pinkus, G. S., Munshi, N., Horner, J., Ivanova, E. V., Protopopov, A., Anderson, K. C., Tonon, G., and DePinho, R. A. (2007) The differentiation and stress response factor XBP-1 drives multiple myeloma pathogenesis. *Cancer Cell* **11**, 349-360

19. Tang, C. H., Ranatunga, S., Kriss, C. L., Cubitt, C. L., Tao, J., Pinilla-Ibarz, J. A., Del Valle, J. R., and Hu, C. C. (2014) Inhibition of ER stress-associated IRE-1/XBP-1 pathway reduces leukemic cell survival. *J Clin Invest* **124**, 2585-2598

20. Harnoss, J. M., Le Thomas, A., Reichelt, M., Guttman, O., Wu, T. D., Marsters, S. A., Shemorry, A., Lawrence, D. A., Kan, D., Segal, E., Merchant, M., Totpal, K., Crocker, L. M., Mesh, K., Dohse, M., Solon, M., Modrusan, Z., Rudolph, J., Koeppen, H., Walter, P., and Ashkenazi, A. (2020) IRE1alpha Disruption in Triple-Negative Breast Cancer Cooperates with Antiangiogenic Therapy by Reversing ER Stress Adaptation and Remodeling the Tumor Microenvironment. *Cancer Res* **80**, 2368-2379

21. Zhao, N., Cao, J., Xu, L., Tang, Q., Dobrolecki, L. E., Lv, X., Talukdar, M., Lu, Y., Wang, X., Hu, D. Z., Shi, Q., Xiang, Y., Wang, Y., Liu, X., Bu, W., Jiang, Y., Li, M., Gong, Y., Sun, Z., Ying, H., Yuan, B., Lin, X., Feng, X. H., Hartig, S. M., Li, F., Shen, H., Chen, Y., Han, L., Zeng, Q., Patterson, J. B., Kaipparettu, B. A., Putluri, N., Sicheri, F., Rosen, J. M., Lewis, M. T., and Chen, X. (2018) Pharmacological targeting of MYC-regulated IRE1/XBP1 pathway suppresses MYC-driven breast cancer. *J Clin Invest* **128**, 1283-1299

22. Chen, X., Iliopoulos, D., Zhang, Q., Tang, Q., Greenblatt, M. B., Hatziapostolou, M., Lim, E., Tam, W. L., Ni, M., Chen, Y., Mai, J., Shen, H., Hu, D. Z., Adoro, S., Hu, B., Song, M., Tan, C., Landis, M. D., Ferrari, M., Shin, S. J., Brown, M., Chang, J. C., Liu,

X. S., and Glimcher, L. H. (2014) XBP1 promotes triple-negative breast cancer by controlling the HIF1alpha pathway. *Nature* **508**, 103-107

23. Li, X. X., Zhang, H. S., Xu, Y. M., Zhang, R. J., Chen, Y., Fan, L., Qin, Y. Q., Liu, Y., Li, M., and Fang, J. (2017) Knockdown of IRE1alpha inhibits colonic tumorigenesis through decreasing beta-catenin and IRE1alpha targeting suppresses colon cancer cells. *Oncogene* **36**, 6738-6746

24. Niederreiter, L., Fritz, T. M., Adolph, T. E., Krismer, A. M., Offner, F. A., Tschurtschenthaler, M., Flak, M. B., Hosomi, S., Tomczak, M. F., Kaneider, N. C., Sarcevic, E., Kempster, S. L., Raine, T., Esser, D., Rosenstiel, P., Kohno, K., Iwawaki, T., Tilg, H., Blumberg, R. S., and Kaser, A. (2013) ER stress transcription factor Xbp1 suppresses intestinal tumorigenesis and directs intestinal stem cells. *J Exp Med* **210**, 2041-2056

25. Zuazo-Gaztelu, I., Lawrence, D., Oikonomidi, I., Marsters, S., Pechuan-Jorge, X., Gaspar, C. J., Kan, D., Segal, E., Clark, K., Beresini, M., Braun, M. G., Rudolph, J., Modrusan, Z., Choi, M., Sandoval, W., Reichelt, M., DeWitt, D. C., Kujala, P., van Dijk, S., Klumperman, J., and Ashkenazi, A. (2025) A nonenzymatic dependency on inositol-requiring enzyme 1 controls cancer cell cycle progression and tumor growth. *PLoS Biol* **23**, e3003086

26. He, S., Fu, T., Yu, Y., Liang, Q., Li, L., Liu, J., Zhang, X., Zhou, Q., Guo, Q., and Xu, D. (2021) IRE1α regulates skeletal muscle regeneration through myostatin mRNA decay. *The Journal of Clinical Investigation* **131**, e143737

27. Roy, A., Tomaz da Silva, M., Bhat, R., Bohnert, K. R., Iwawaki, T., and Kumar, A. (2021) The IRE1/XBP1 signaling axis promotes skeletal muscle regeneration through a cell non-autonomous mechanism. *Elife* **10**, e73215

28. Joshi, A. S., Castillo, M. B., Tomaz da Silva, M., Vuong, A. T., Gunaratne, P. H., Darabi, R., Liu, Y., and Kumar, A. (2024) Single-nucleus transcriptomic analysis reveals the regulatory circuitry of myofiber XBP1 during regenerative myogenesis. *iScience* **27**, 111372

29. Joshi, A. S., Tomaz da Silva, M., Roy, A., Koike, T. E., Wu, M., Castillo, M. B., Gunaratne, P. H., Liu, Y., Iwawaki, T., and Kumar, A. (2024) The IRE1alpha/XBP1 signaling axis drives myoblast fusion in adult skeletal muscle. *EMBO Rep* **25**, 3627-3650

30. Hetz, C., Axten, J. M., and Patterson, J. B. (2019) Pharmacological targeting of the unfolded protein response for disease intervention. *Nature chemical biology* **15**, 764-775

31. Ketelut-Carneiro, N., and Fitzgerald, K. A. (2022) Apoptosis, Pyroptosis, and Necroptosis-Oh My! The Many Ways a Cell Can Die. *J Mol Biol* **434**, 167378

32. Avril, T., Vauleon, E., and Chevet, E. (2017) Endoplasmic reticulum stress signaling and chemotherapy resistance in solid cancers. *Oncogenesis* **6**, e373

33. Bisogno, G., De Salvo, G. L., Bergeron, C., Gallego Melcon, S., Merks, J. H., Kelsey, A., Martelli, H., Minard-Colin, V., Orbach, D., Glosli, H., Chisholm, J., Casanova, M., Zanetti, I., Devalck, C., Ben-Arush, M., Mudry, P., Ferman, S., Jenney, M., Ferrari, A., and European paediatric Soft tissue sarcoma Study, G. (2019) Vinorelbine and continuous low-dose cyclophosphamide as maintenance chemotherapy in patients with high-risk rhabdomyosarcoma (RMS 2005): a multicentre, open-label, randomised, phase 3 trial. *Lancet Oncol* **20**, 1566-1575

34. Miwa, S., Yamamoto, N., Hayashi, K., Takeuchi, A., Igarashi, K., and Tsuchiya, H. (2020) Recent Advances and Challenges in the Treatment of Rhabdomyosarcoma. *Cancers (Basel)* **12**

35. Al-Hajj, M., Wicha, M. S., Benito-Hernandez, A., Morrison, S. J., and Clarke, M. F. (2003) Prospective identification of tumorigenic breast cancer cells. *Proc Natl Acad Sci U S A* **100**, 3983-3988

36. Pattabiraman, D. R., and Weinberg, R. A. (2014) Tackling the cancer stem cells - what challenges do they pose? *Nat Rev Drug Discov* **13**, 497-512

37. Medema, J. P. (2013) Cancer stem cells: the challenges ahead. *Nat Cell Biol* **15**, 338-344

38. Zhao, W., Li, Y., and Zhang, X. (2017) Stemness-Related Markers in Cancer. *Cancer Transl Med* **3**, 87-95

39. Generali, M., Satheesha, S., Bode, P. K., Wanner, D., Schafer, B. W., and Casanova, E. A. (2021) High Frequency of Tumor Propagating Cells in Fusion-Positive Rhabdomyosarcoma. *Genes (Basel)* **12**

40. Radzikowska, J., Czarnecka, A. M., Klepacka, T., Rychlowska-Pruszynska, M., Raciborska, A., Dembowska-Baginska, B., Pronicki, M., Kukwa, A., Fendler, W., Smyczynska, U., Kukwa, W., and Krzeski, A. (2022) Cancer Stem Cell Markers in Rhabdomyosarcoma in Children. *Diagnostics (Basel)* **12**

41. Slemmons, K. K., Crose, L. E. S., Riedel, S., Sushnitha, M., Belyea, B., and Linardic, C. M. (2017) A Novel Notch-YAP Circuit Drives Stemness and Tumorigenesis in Embryonal Rhabdomyosarcoma. *Mol Cancer Res* **15**, 1777-1791

42. Slemmons, K. K., Deel, M. D., Lin, Y. T., Oristian, K. M., Kuprasertkul, N., Genadry, K. C., Chen, P. H., Chi, J. T., and Linardic, C. M. (2021) A method to culture human alveolar rhabdomyosarcoma cell lines as rhabdospheres demonstrates an enrichment in stemness and Notch signaling. *Biol Open* **10**

43. Walter, D., Satheesha, S., Albrecht, P., Bornhauser, B. C., D'Alessandro, V., Oesch, S. M., Rehrauer, H., Leuschner, I., Koscielniak, E., Gengler, C., Moch, H., Bernasconi, M., Niggli, F. K., Schafer, B. W., and Group, C. W. S. S. (2011) CD133 positive embryonal rhabdomyosarcoma stem-like cell population is enriched in rhabdospheres. *PLoS One* **6**, e19506

44. Nachiyappan, A., Soon, J. L. J., Lim, H. J., Lee, V. K., and Taneja, R. (2022) EHMT1 promotes tumor progression and maintains stemness by regulating ALDH1A1 expression in alveolar rhabdomyosarcoma. *J Pathol* **256**, 349-362

45. Bach, D. H., Park, H. J., and Lee, S. K. (2018) The Dual Role of Bone Morphogenetic Proteins in Cancer. *Mol Ther Oncolytics* **8**, 1-13

46. Cuny, G. D., Yu, P. B., Laha, J. K., Xing, X., Liu, J. F., Lai, C. S., Deng, D. Y., Sachidanandan, C., Bloch, K. D., and Peterson, R. T. (2008) Structure-activity relationship study of bone morphogenetic protein (BMP) signaling inhibitors. *Bioorg Med Chem Lett* **18**, 4388-4392

47. Skapek, S. X., Ferrari, A., Gupta, A. A., Lupo, P. J., Butler, E., Shipley, J., Barr, F. G., and Hawkins, D. S. (2019) Rhabdomyosarcoma. *Nat Rev Dis Primers* **5**, 1

48. Urra, H., Dufey, E., Avril, T., Chevet, E., and Hetz, C. (2016) Endoplasmic Reticulum Stress and the Hallmarks of Cancer. *Trends Cancer* **2**, 252-262

49. Zhang, W., Shi, Y., Oyang, L., Cui, S., Li, S., Li, J., Liu, L., Li, Y., Peng, M., Tan, S., Xia, L., Lin, J., Xu, X., Wu, N., Peng, Q., Tang, Y., Luo, X., Liao, Q., Jiang, X., and Zhou, Y. (2024) Endoplasmic reticulum stress-a key guardian in cancer. *Cell Death Discov* **10**, 343

50. Sheng, X., Nenseth, H. Z., Qu, S., Kuzu, O. F., Frahnow, T., Simon, L., Greene, S., Zeng, Q., Fazli, L., Rennie, P. S., Mills, I. G., Danielsen, H., Theis, F., Patterson, J. B., Jin, Y., and Saatcioglu, F. (2019) IRE1alpha-XBP1s pathway promotes prostate cancer by activating c-MYC signaling. *Nat Commun* **10**, 323

51. Tameire, F., Verginadis, II, and Koumenis, C. (2015) Cell intrinsic and extrinsic activators of the unfolded protein response in cancer: Mechanisms and targets for therapy. *Semin Cancer Biol* **33**, 3-15

52. Lhomond, S., Avril, T., Dejeans, N., Voutetakis, K., Doultsinos, D., McMahon, M., Pineau, R., Obacz, J., Papadodima, O., Jouan, F., Bourien, H., Logotheti, M., Jegou, G., Pallares-Lupon, N., Schmit, K., Le Reste, P. J., Etcheverry, A., Mosser, J., Barroso, K., Vauleon, E., Maurel, M., Samali, A., Patterson, J. B., Pluquet, O., Hetz, C., Quillien, V., Chatziioannou, A., and Chevet, E. (2018) Dual IRE1 RNase functions dictate glioblastoma development. *EMBO Mol Med* **10**

53. Cubillos-Ruiz, J. R., Bettigole, S. E., and Glimcher, L. H. (2017) Tumorigenic and Immunosuppressive Effects of Endoplasmic Reticulum Stress in Cancer. *Cell* **168**, 692-706

54. McCarthy, N., Dolgikh, N., Logue, S., Patterson, J. B., Zeng, Q., Gorman, A. M., Samali, A., and Fulda, S. (2020) The IRE1 and PERK arms of the unfolded protein response promote survival of rhabdomyosarcoma cells. *Cancer Lett* **490**, 76-88

55. Logue, S. E., McGrath, E. P., Cleary, P., Greene, S., Mnich, K., Almanza, A., Chevet, E., Dwyer, R. M., Oommen, A., Legembre, P., Godey, F., Madden, E. C., Leuzzi, B., Obacz, J., Zeng, Q., Patterson, J. B., Jager, R., Gorman, A. M., and Samali, A. (2018) Inhibition of IRE1 RNase activity modulates the tumor cell secretome and enhances response to chemotherapy. *Nat Commun* **9**, 3267

56. Xu, Y., Gui, F., Zhang, Z., Chen, Z., Zhang, T., Hu, Y., Wei, H., Fu, Y., Chen, X., and Wu, Z. (2024) IRE1alpha-XBP1s axis regulates SREBP1-dependent MRP1 expression to promote chemoresistance in non-small cell lung cancer cells. *Thorac Cancer* **15**, 2116-2127

57. Li, Y., Lu, L., Zhang, G., Ji, G., and Xu, H. (2022) The role and therapeutic implication of endoplasmic reticulum stress in inflammatory cancer transformation. *Am J Cancer Res* **12**, 2277-2292

58. Hettmer, S., Li, Z., Billin, A. N., Barr, F. G., Cornelison, D. D., Ehrlich, A. R., Guttridge, D. C., Hayes-Jordan, A., Helman, L. J., Houghton, P. J., Khan, J., Langenau, D. M., Linardic, C. M., Pal, R., Partridge, T. A., Pavlath, G. K., Rota, R., Schafer, B. W., Shipley, J., Stillman, B., Wexler, L. H., Wagers, A. J., and Keller, C. (2014) Rhabdomyosarcoma: current challenges and their implications for developing therapies. *Cold Spring Harb Perspect Med* **4**, a025650

59. Ono, Y., Calhabeu, F., Morgan, J. E., Katagiri, T., Amthor, H., and Zammit, P. S. (2011) BMP signalling permits population expansion by preventing premature myogenic differentiation in muscle satellite cells. *Cell Death Differ* **18**, 222-234

60. Frank, N. Y., Kho, A. T., Schatton, T., Murphy, G. F., Molloy, M. J., Zhan, Q., Ramoni, M. F., Frank, M. H., Kohane, I. S., and Gussoni, E. (2006) Regulation of myogenic progenitor proliferation in human fetal skeletal muscle by BMP4 and its antagonist Gremlin. *J Cell Biol* **175**, 99-110

61. Voeltzel, T., Flores-Violante, M., Zylbersztejn, F., Lefort, S., Billandon, M., Jeanpierre, S., Joly, S., Fossard, G., Milenkov, M., Mazurier, F., Nehme, A., Belhabri, A., Paubelle, E., Thomas, X., Michallet, M., Louache, F., Nicolini, F. E., Caron de Fromentel, C., and Maguer-Satta, V. (2018) A new signaling cascade linking BMP4, BMPR1A, DeltaNp73 and NANOG impacts on stem-like human cell properties and patient outcome. *Cell Death Dis* **9**, 1011

62. Pickup, M. W., Hover, L. D., Guo, Y., Gorska, A. E., Chytil, A., Novitskiy, S. V., Moses, H. L., and Owens, P. (2015) Deletion of the BMP receptor BMPR1a impairs mammary tumor formation and metastasis. *Oncotarget* **6**, 22890-22904

63. Tomaz da Silva, M., Roy, A., Vuong, A. T., Joshi, A. S., Josphien, C., Trivedi, M. V., Hindi, S. M., Narkar, V. A., and Kumar, A. (2025) The TWEAK/Fn14 signaling mediates skeletal muscle wasting during cancer cachexia. *iScience* **28**, 112714

64. Zhou, Y., Zhou, B., Pache, L., Chang, M., Khodabakhshi, A. H., Tanaseichuk, O., Benner, C., and Chanda, S. K. (2019) Metascape provides a biologist-oriented resource for the analysis of systems-level datasets. *Nat Commun* **10**, 1523

65. Tomaz da Silva, M., Joshi, A. S., Castillo, M. B., Koike, T. E., Roy, A., Gunaratne, P. H., and Kumar, A. (2023) Fn14 promotes myoblast fusion during regenerative myogenesis. *Life Sci Alliance* **6**

66. Gu, Z., and Hubschmann, D. (2022) Make Interactive Complex Heatmaps in R. *Bioinformatics* **38**, 1460-1462

FIGURES and LEGENDS

FIGURE 1

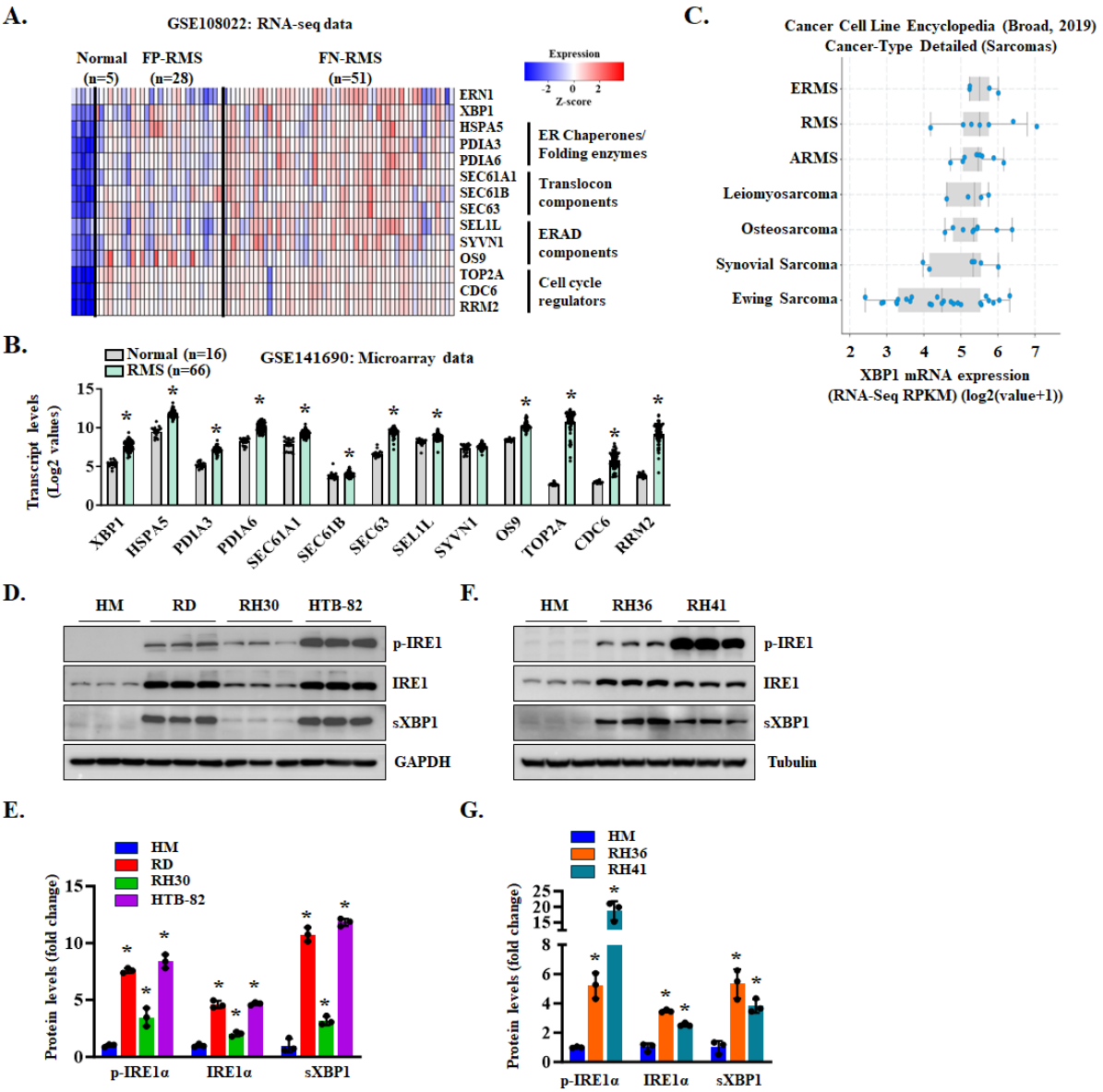

FIGURE 1. IRE1α/XBP1 signaling is activated in RMS patient tumor samples and cell lines. (A) Heatmap representing relative mRNA levels of IRE1α (gene name: *ERN1*), XBP1 and known XBP1-target genes in human skeletal muscle tissue (normal), fusion-positive RMS (FP-RMS), and fusion-negative RMS (FN-RMS) tumor specimens analyzed using a publicly available RNA-seq dataset (GSE108022). n=5, 28, and 51 for normal, FP-RMS and FN-RMS, respectively. Data are presented as z-scores calculated from Log2(FPKM+1) values. **(B)** Transcript levels of XBP1 and its target genes in normal human skeletal muscle tissue (n=16) and RMS tumors (n=66) analyzed using publicly available GSE141690 microarray dataset. Data are presented as mean ± SEM. *p<0.05, values significantly different from normal muscle analyzed by unpaired Student *t* test. **(C)** Box plot showing mRNA levels of XBP1 in different sarcoma cell lines analyzed using the Cancer Cell Line Encyclopedia (Broad, 2019) database on

cBioPortal website. **(D)** Immunoblots and **(E)** densitometry analysis showing the levels of phosphorylated IRE1α (p-IRE1α), total IRE1α, and spliced XBP1 (sXBP1) protein in human myoblasts (HM), and RD, RH30, and HTB82 cell lines. n=3 per group. Data are presented as mean ± SD. *$p<0.05$, values significantly different from HM analyzed by unpaired Student *t* test. **(F)** Immunoblots and **(G)** densitometry analysis showing the expression levels of phosphorylated IRE1α (p-IRE1α), total IRE1α, and spliced XBP1 (sXBP1) protein in HM, RH36 and RH41 cell lines. n=3 per group. Data are presented as mean ± SD. *$p<0.05$, values significantly different from HM analyzed by unpaired Student *t* test.

FIGURE 2

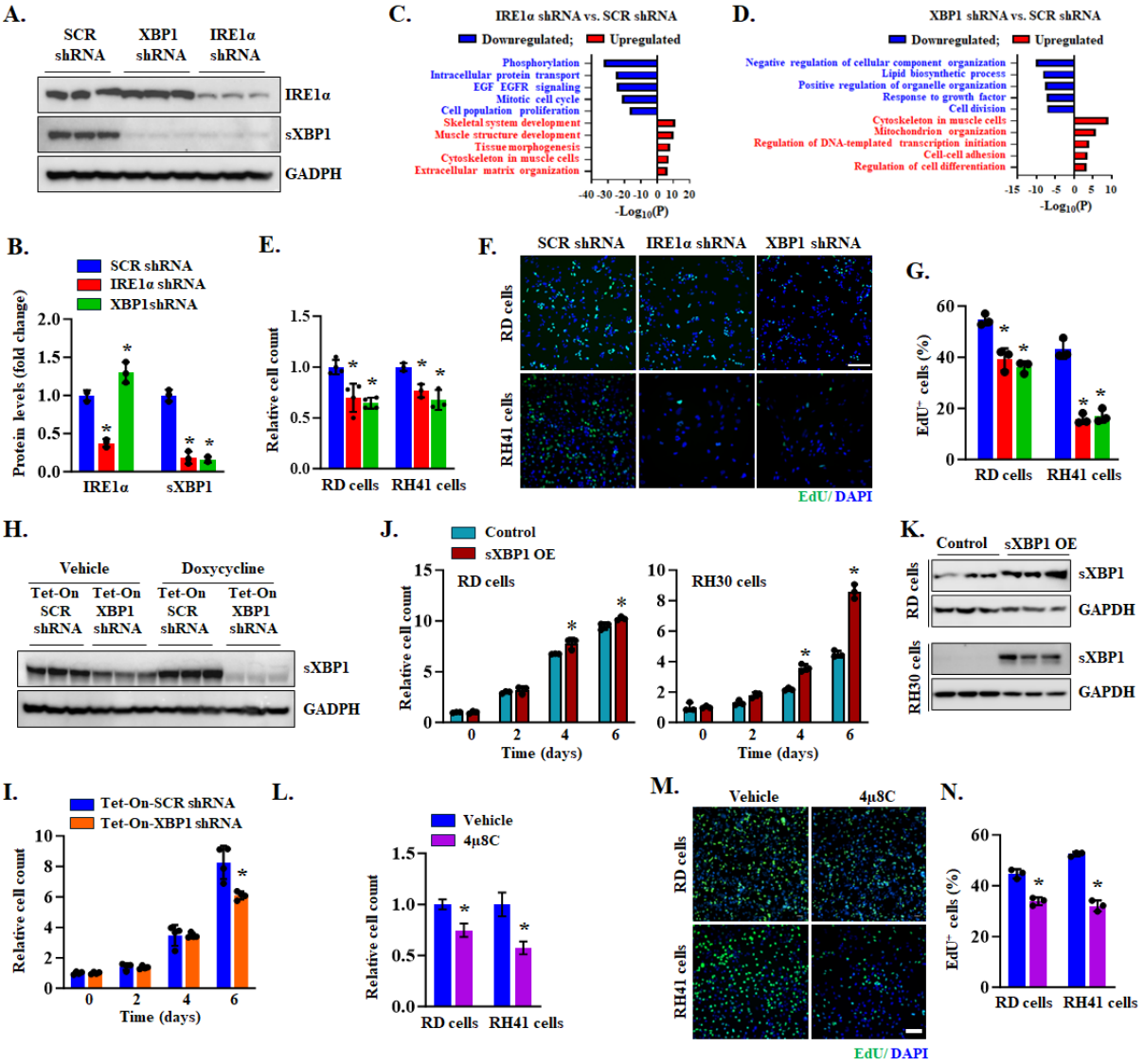

FIGURE 2. Inhibition of IRE1α/XBP1 signaling reduces proliferation of RMS cell lines. **(A)** Immunoblots and **(B)** densitometry analysis showing the levels of IRE1α and spliced XBP1 (sXBP1) protein in scrambled (SCR), XBP1 or IRE1α shRNA expressing RD cultures. n=3 per group. Data are presented as mean ± SD. *p<0.05, values significantly different from SCR cultures analyzed by unpaired Student *t* test. **(C, D)** Bulk RNA-seq analysis of RD cells stably expressing SCR, IRE1α or XBP1 shRNA was performed followed by identifying differentially expressed genes (DEGs) and pathway enrichment analysis using Metascape Annotation Tool. Bar plots show enriched pathways associated with upregulated and downregulated genes in RD cells expressing **(C)** IRE1α shRNA and **(D)** XBP1 shRNA compared with those expressing SCR shRNA. **(E)** Relative cell count analyzed after 5 days of culturing SCR, IRE1α or XBP1 shRNA expressing RD and RH41 cells. n=3 per group. Data are presented as mean ± SD. *p<0.05, values significantly different from SCR cultures analyzed by unpaired Student *t* test. **(F, G)** RD and RH41 cells stably expressing SCR, IRE1α, or XBP1 shRNA were seeded at equal densities and incubated in growth media for 48 h, followed EdU incorporation for 2 h. **(F)** Representative

photomicrographs after EdU detection. Scale bar, 100µm. **(G)** Quantification of proportion of EdU^+ cells in IRE1α- or XBP1-knockdown RD and RH41 cultures compared with corresponding control cultures. n=3 per group. Data are presented as mean ± SD. *p<0.05, values significantly different from SCR cultures analyzed by unpaired Student *t* test. **(H)** Immunoblots showing levels of spliced XBP1 (sXBP1) protein in RD cells expressing inducible (Tet-On) SCR or XBP1 shRNA after 72 h treatment with doxycycline or vehicle alone. n=3 per group. **(I)** Relative number of RD cells expressing Tet-On-SCR or -XBP1 shRNA at indicated time points after treatment with doxycycline or vehicle alone. n=4 per group. Data are presented as mean ± SD. *p<0.05, values significantly different from RD cells expressing Tet-On SCR shRNA analyzed by unpaired Student *t* test. **(J)** Relative number of RD and RH30 cells stably expressing Tet-On sXBP1 cDNA at indicated time points after treatment with doxycycline (sXBP1 OE) or vehicle alone (Control). n=4 per group. Data are presented as mean ± SD. *p<0.05, values significantly different from control cultures analyzed by unpaired Student *t* test. **(K)** Immunoblots showing levels of sXBP1 protein in control and sXBP1 OE RD and RH30 cultures. n=3 per group. **(L)** Relative number of RD and RH41 cells after 5 days treatment with 10 µM 4µ8C or vehicle alone. n=4 per group. Data are presented as mean ± SD. *p<0.05, values significantly different from RD or RH41 cells treated with vehicle alone analyzed by unpaired Student *t* test. **(M)** Representative photomicrographs after EdU detection. Scale bar, 100 µm. **(N)** Quantification of proportion of EdU^+ cells in RD and RH41 cultures treated with 4µ8C or vehicle alone. n=3 per group. Data are presented as mean ± SD. *p<0.05, values significantly different from corresponding vehicle-treated cultures analyzed by unpaired Student *t* test.

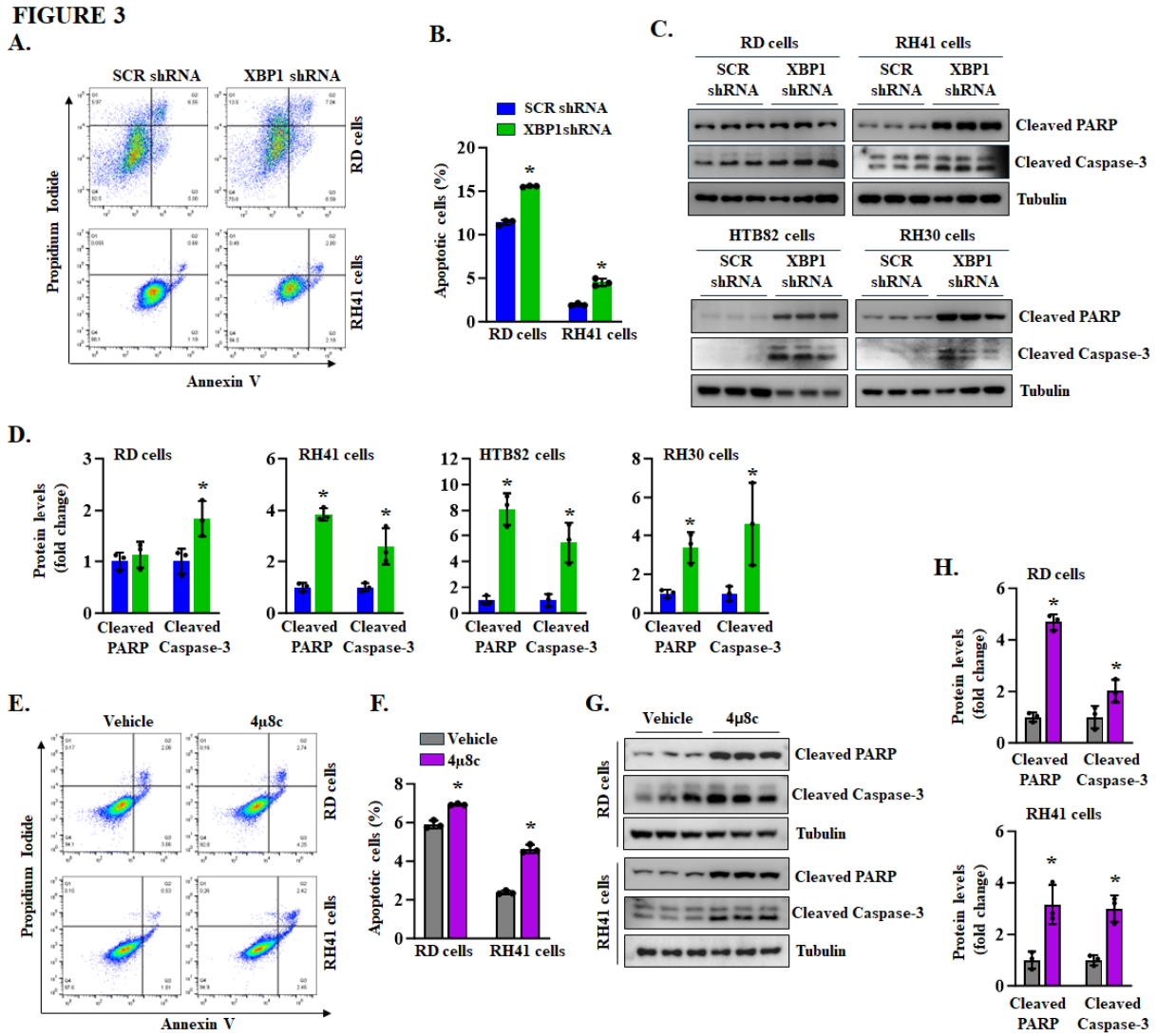

FIGURE 3. Silencing of IRE1α/XBP1 signaling promotes apoptosis in RMS cells. (A, B) RD and RH41 cells were transduced with lentivirus SCR or XBP1 shRNA. After 5 days, the cells were analyzed for apoptosis using propidium iodide (PI) and Annexin V staining, followed by FACS analysis. **(A)** Scatter plots and **(B)** proportion of apoptotic cells in XBP1-knockdown RD and RH41 cells compared with corresponding control cultures expressing SCR shRNA. n=3 per group. Data are presented as mean ± SD. *p<0.05, values significantly different from corresponding cultures expressing SCR shRNA analyzed by unpaired Student *t* test. **(C)** Immunoblots and **(D)** densitometry analysis showing levels of cleaved PARP and cleaved Caspase-3 protein in SCR or XBP1 shRNA expressing RD, RH41, HTB82, and RH30 cultures. n=3 per group. Data are presented as mean ± SD. *p<0.05, values significantly different from corresponding cultures expressing SCR shRNA analyzed by unpaired Student *t* test. **(E, F)** RD and RH41 cells were treated with 10 μM 4μ8C or vehicle alone for 3 days, followed by staining with PI and Annexin V and FACS analysis. **(E)** Scatter plots, and **(F)** quantification of proportion of apoptotic cells in vehicle- or 4μ8C-treated RD and RH41 cells. n=3 per group. Data are presented as mean ± SD. *p<0.05, values significantly different from corresponding vehicle-treated cultures analyzed by unpaired Student *t* test. **(G)** Immunoblots, and **(H)** densitometry

analysis showing levels of cleaved PARP and cleaved caspase-3 protein in RD and RH41 cultures treated with 4μ8C or vehicle alone. n=3 per group. Data are presented as mean ± SD. *$p<0.05$, values significantly different from vehicle-treated cultures analyzed by unpaired Student *t* test

FIGURE 4

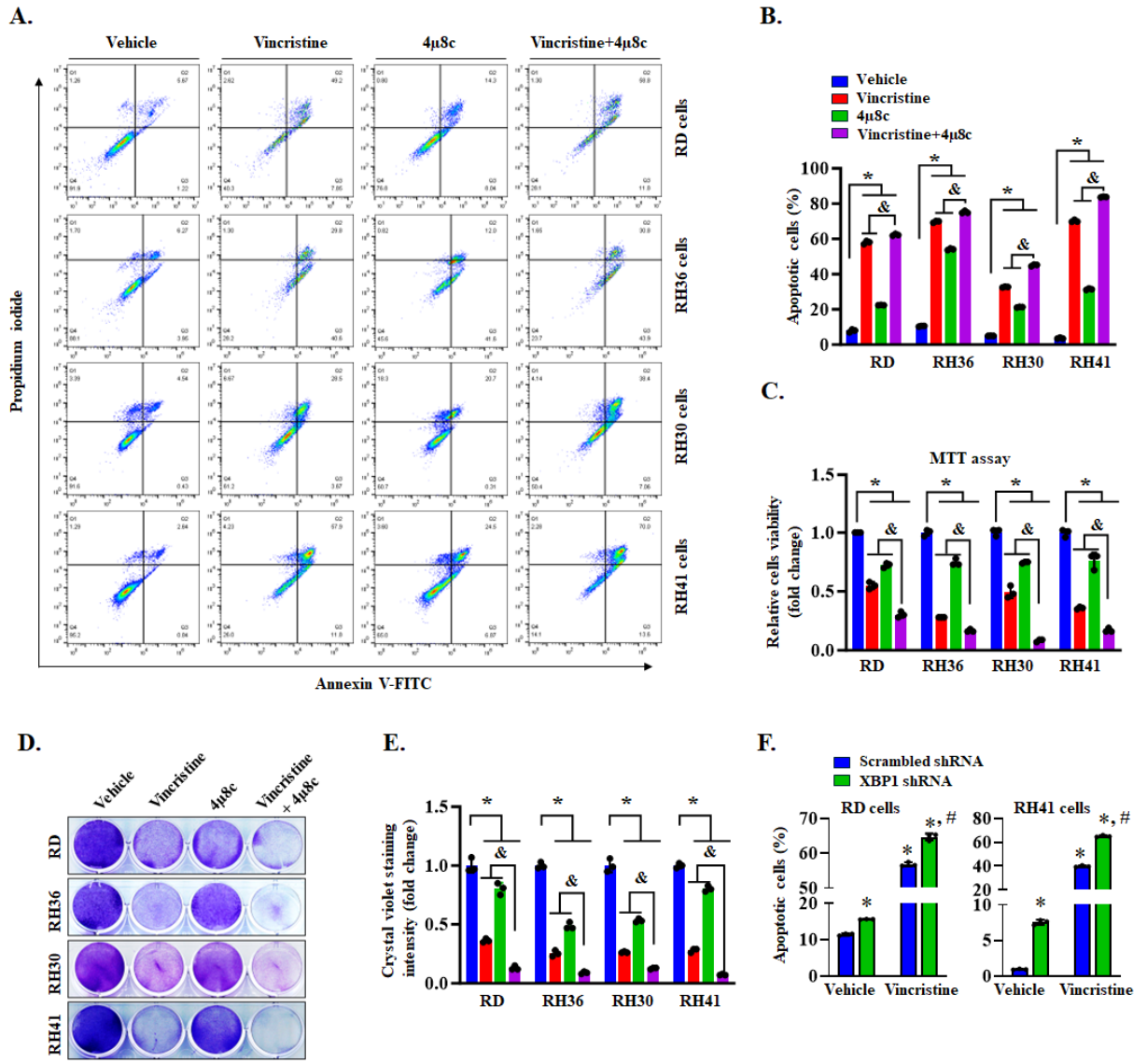

FIGURE 4. Pharmacological inhibition of IRE1α/XBP1 axis potentiates vincristine-induced cell death in RMS cultures. RD, RH36, RH30, and RH41 cells were treated with vehicle, vincristine (1nM for RH41 cells; 2nM for RD, RH36, RH30 cells), 10μM 4μ8C, or a combination of vincristine and 4μ8C for 5 days, followed by staining with propidium iodide and Annexin V and FACS analysis. **(A)** Scatter plots and **(B)** quantification of proportion of apoptotic cells in cultures treated with vehicle alone, vincristine, 4μ8C, or combination of vincristine and 4μ8C. n=3 per group. Data are presented as mean ± SD. *$p<0.05$, values significantly different from corresponding vehicle-treated cultures; $^{\&}p<0.05$, values significantly different from corresponding vincristine-treated cultures analyzed by unpaired Student *t* test. **(C)** Relative viability in RD, RH36, RH30, and RH41 cells after treatment with vehicle, vincristine, 4μ8C, or a combination of vincristine and 4μ8C for 5 days, assayed by performing MTT assay. n=3 per group. Data are presented as mean ± SD. *$p<0.05$, values significantly different from corresponding vehicle-treated cultures; $^{\&}p<0.05$, values significantly different from corresponding vincristine-treated cultures analyzed by unpaired Student *t* test. **(D)**

Representative images of wells after staining with crystal violet dye. **(E)** Quantification of crystal violet staining intensity in RD, RH36, RH30, and RH41 cells after treatment with vehicle, vincristine, 4μ8C, or a combination of vincristine and 4μ8C for 5 days. n=3 per group. Data are presented as mean ± SD. *$p<0.05$, values significantly different from corresponding vehicle-treated cultures; $^{\&}p<0.05$, values significantly different from corresponding combination of 4μ8C and vincristine-treated cultures analyzed by unpaired Student *t* test. **(F)** Control and XBP1 knockdown RD and RH41 cells were treated with vincristine (2 nM RD and 1 nM RH41) or vehicle alone and the percentage of apoptotic cells were determined by performing Annexin V staining and FACS analysis. *$p<0.05$, values significantly different from vehicle-treated cultures expressing scrambled (SCR) shRNA. $^{\#}p<0.05$, values significantly different from corresponding vincristine-treated cultures expressing SCR.

FIGURE 5

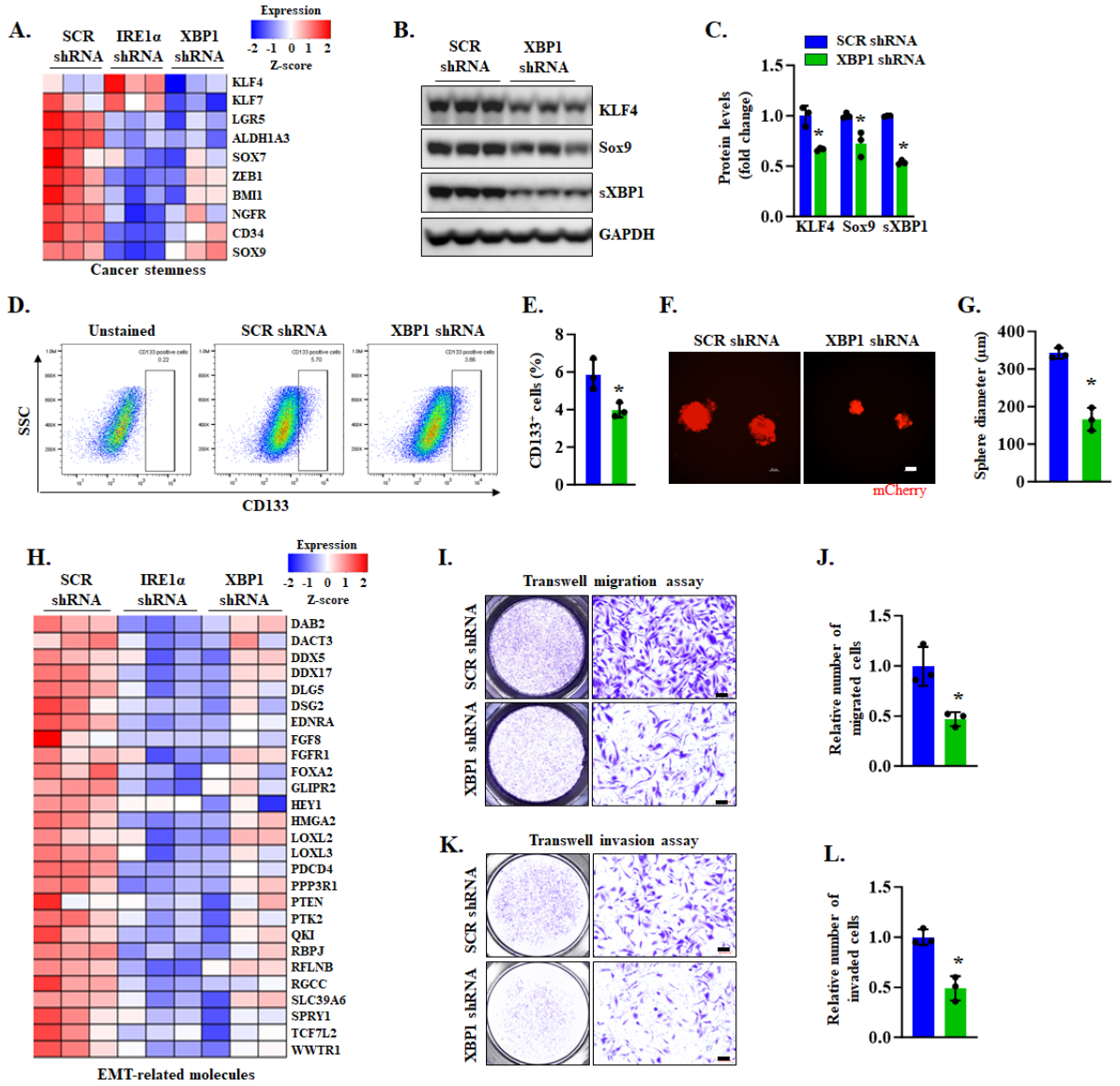

FIGURE 5. Inhibition of IRE1α/XBP1 axis represses stemness and EMT phenotype in RD cultures. (A) Heatmap represents relative mRNA levels of various cancer stemness-related molecules in RD cultures stably expressing scrambled (SCR), IRE1α, or XBP1 shRNA analyzed from RNA-seq dataset. **(B)** Immunoblots, and **(C)** densitometry analysis of levels of KLF4, Sox9 and sXBP1 protein in RD cultures stably expressing XBP1 shRNA compared with control cultures expressing SCR shRNA. n=3 per group. Data are presented as mean ± SD. *p<0.05, values significantly different from SCR shRNA-expressing RD cultures analyzed by unpaired Student *t* test. **(D)** Scatter plot, and **(E)** quantification of $CD133^+$ cells in RD cultures stably expressing SCR or XBP1 shRNA after performing FACS analysis. n=3 per group. Data are presented as mean ± SD. *p<0.05, values significantly different from SCR shRNA-expressing RD cultures analyzed by unpaired Student *t* test. Data are presented as mean ± SD. *p<0.05, values significantly different from SCR shRNA-expressing RD cultures analyzed by unpaired Student *t* test. **(F)** Representative images of spheres. Scale bar, 100μm. **(G)** Quantification of average diameter of RD spheres stably expressing SCR or XBP1 shRNA. n=3 per group. Data

are presented as mean ± SD. *p<0.05, values significantly different from SCR shRNA-expressing RD cultures analyzed by unpaired Student *t* test. **(H)** Heatmap generated from RNA-seq dataset analysis shows relative transcript levels of various EMT-related genes in RD cultures stably expressing SCR, IRE1α, or XBP1 shRNA. **(I)** Representative images of migration assay. Scale bar, 100μm. **(J)** Quantification of number of migrated control and XBP1 knockdown RD cells. n=3 per group. Data are presented as mean ± SD. *p<0.05, values significantly different from SCR shRNA-expressing RD cultures analyzed by unpaired Student *t* test. **(K)** Representative images of invasion assay. Scale bar, 100μm. **(L)** Quantification of number of invaded cells in control and XBP1 knockdown RD cultures. n=3 per group. Data are presented as mean ± SD. *p<0.05, values significantly different from SCR shRNA-expressing RD cultures analyzed by unpaired Student *t* test.

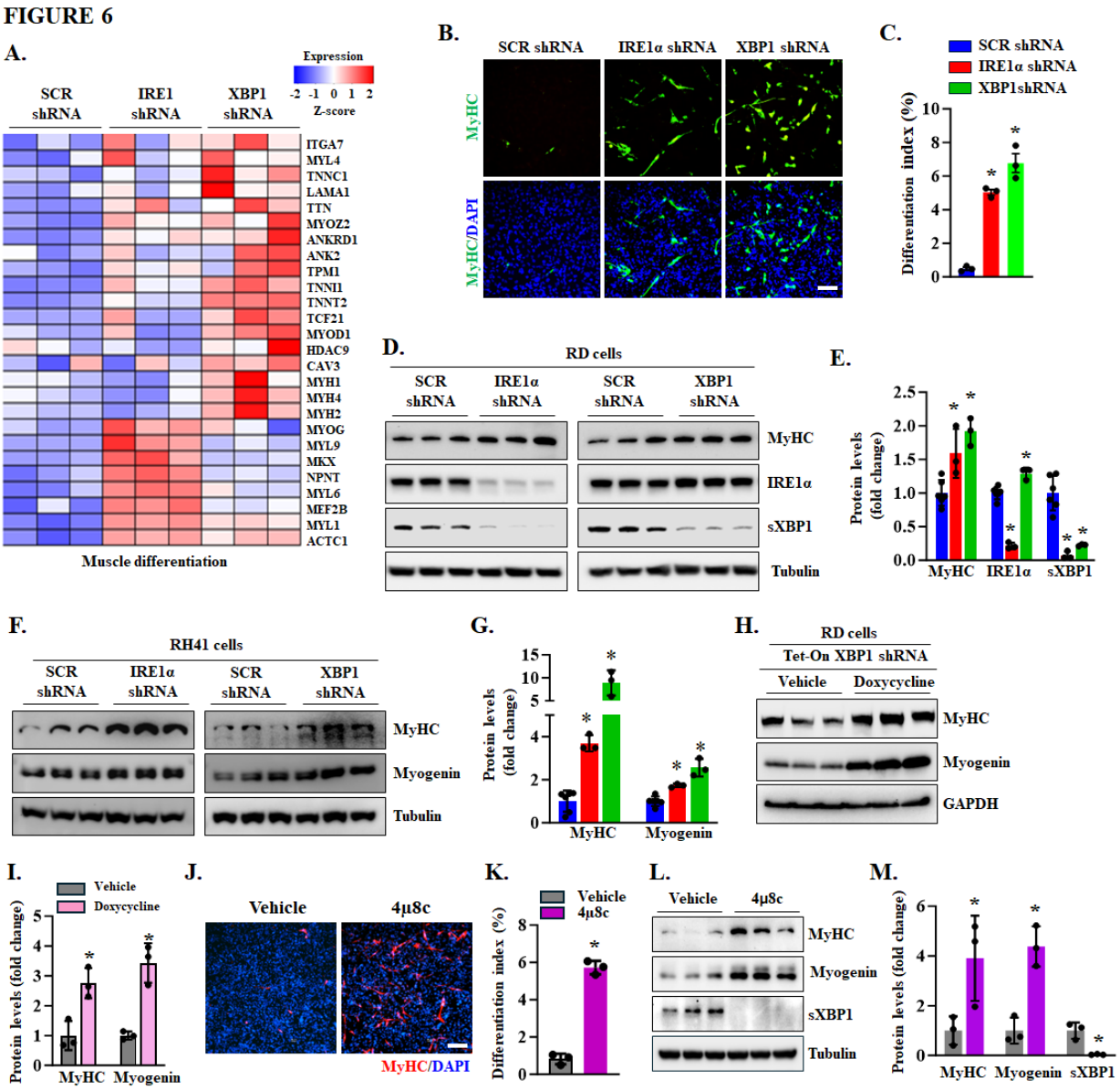

FIGURE 6. Silencing of IRE1α/XBP1 signaling axis promotes differentiation in RMS cell lines. (A) Heatmap generated from RNA-Seq dataset show relative mRNA levels of various muscle differentiation-related molecules in RD cultures stably expressing scrambled (SCR), IRE1α, or XBP1 shRNA. **(B)** RD cells stably expressing SCR, IRE1α, or XBP1 shRNA were plated at equal density and analyzed at 5 days by immunostaining for myosin heavy chain (MyHC) protein. DAPI was used to counterstain nuclei. Representative photomicrographs of MyHC-stained cultures are presented here. Scale bar, 100μm. **(C)** Quantification of differentiation index in RD cultures expressing SCR, IRE1α or XBP1 shRNA and immunostained for MyHC. n=3 per group. Data are presented as mean ± SD. *p<0.05, values significantly different from SCR shRNA-expressing RD cultures analyzed by unpaired Student *t* test. **(D)** Immunoblots, and **(E)** densitometry analysis of levels of MyHC, IRE1α and sXBP1 protein in SCR, IRE1α or XBP1 shRNA expressing RD cultures. n=6 (SCR shRNA) and 3 (IRE1α or XBP1 shRNA). Data are presented as mean ± SD. *p<0.05, values significantly different from SCR shRNA-expressing RD cultures analyzed by unpaired Student *t* test. **(F)**

Immunoblots, and **(G)** densitometry analysis of MyHC and myogenin protein levels in RH41 cells stably expressing SCR, IRE1α, or XBP1shRNA. n=6 (SCR shRNA) and 3 (IRE1α or XBP1 shRNA). Data are presented as mean ± SD. *p<0.05, values significantly different from SCR shRNA-expressing RD cultures analyzed by unpaired Student *t* test. **(H)** Immunoblots and **(I)** densitometry analysis of levels of MyHC and myogenin protein in RD cultures expressing Tet-On XBP1 shRNA after 5 days treatment with doxycycline or vehicle alone. n=3 per group. Data are presented as mean ± SD. *p<0.05, values significantly different from vehicle-treated RD cultures expressing Tet-On XBP1 shRNA analyzed by unpaired Student *t* test. **(J)** RD cells were incubated in growth media for 72 h with vehicle alone or 10μM 4μ8C followed by performing anti-MyHC and DAPI staining. Representative photomicrographs of MyHC-stained cultures are presented here. Scale bar, 100μm. **(K)** Quantification of differentiation index analyzed from MyHC-stained RD cultures treated with vehicle or 4μ8C. n=3 per group. Data are presented as mean ± SD. *p<0.05, values significantly different from vehicle-treated RD cultures analyzed by unpaired Student *t* test. **(L)** Immunoblots, and **(M)** densitometry analysis of levels of MyHC, myogenin, and sXBP1 protein in RD cultures after 72 h of treatment with 4μ8C or vehicle alone. n=3 per group. Data are presented as mean ± SD. *p<0.05, values significantly different from vehicle-treated RD cultures analyzed by unpaired Student *t* test.

FIGURE 7

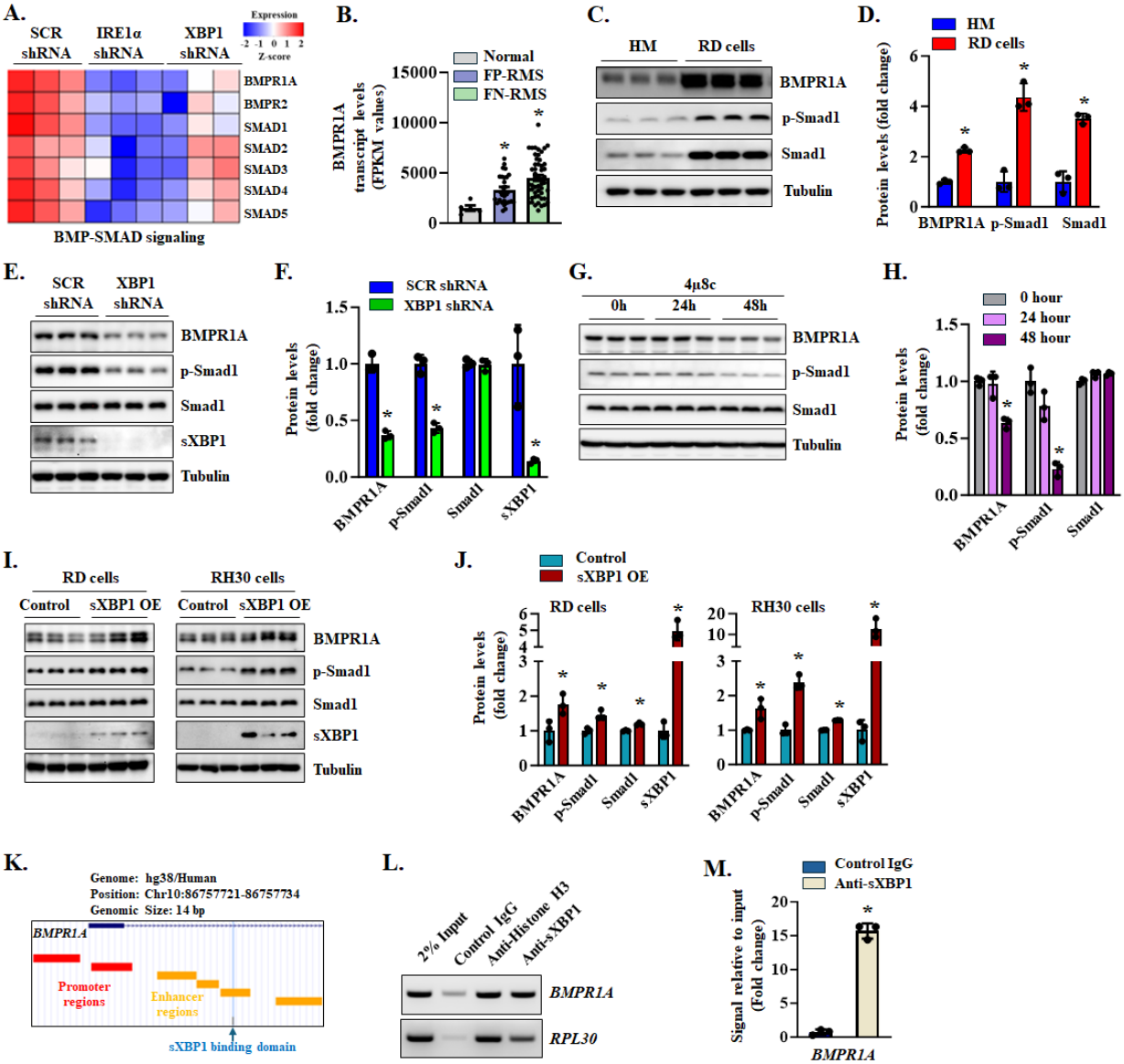

FIGURE 7. IRE1α/XBP1 signaling regulates BMPR1A expression in RMS cells. (A) Heatmap generated from RNA-seq dataset show relative mRNA levels of multiple BMP-SMAD signaling-related molecules in RD cultures stably expressing scrambled (SCR), IRE1α, or XBP1 shRNA. **(B)** Bar plot shows transcript levels of BMPR1A in human skeletal muscle tissue (Normal), and fusion positive and fusion negative RMS (i.e., FP-RMS and FN-RMS, respectively) patient tumor specimens obtained by analyzing a publicly available RNA-seq database (GSE108022). **(C)** Immunoblots and **(D)** densitometry analysis showing the levels of BMPR1A, phosphorylated Smad1 (p-Smad1), and total Smad1 protein in human myoblasts (HM) and RD cultures . n=3 per group. Data are presented as mean ± SD. *p<0.05, values significantly different from HM analyzed by unpaired Student *t* test. **(E)** Immunoblots and **(F)** densitometry analysis of levels of BMPR1A, p-Smad1, total Smad1, and sXBP1 protein in RD cultures stably expressing SCR or XBP1 shRNA. n=3 per group. Data are presented as mean ± SD. *p<0.05, values significantly different from SCR shRNA-expressing RD cultures analyzed

by unpaired Student *t* test. **(G)** Immunoblots and **(H)** densitometry analysis of levels of BMPR1A, p-Smad1, and total Smad1 protein in RD cultures after treatment with 10μM 4μ8C for indicated time points. n=3 per group. Data are presented as mean ± SD. *$p<0.05$, values significantly different from untreated (0 hour) RD cultures analyzed by unpaired Student *t* test. RD and RH30 cells stably expressing Tet-On sXBP1 cDNA were treated with doxycycline (sXBP1 OE) or vehicle alone (Control) for 5 days. **(I)** Immunoblots and **(J)** densitometry analysis of levels of BMPR1A, p-Smad1, total Smad1, and sXBP1 protein in control and sXBP1 OE RD and RH30 cultures. n=3 per group. Data are presented as mean ± SD. *$p<0.05$, values significantly different from control cultures analyzed by unpaired Student *t* test. **(K)** Schematic representation of the promoter/enhancer regions flanking the transcription start site of *BMPR1A* gene. Chromatin immunoprecipitation (ChIP) assay was performed using RD cells, followed by semi-quantitative and quantitative PCR using primers designed to amplify ~150 bp region containing the identified sXBP1 binding domain on the enhancer region of *BMPR1A* gene. **(L)** Agarose gel image shows the binding of sXBP1 protein to the promoter of *BMPR1A* gene. Validation of ChIP assay was performed using PCR for Histone H3 antibody binding to the promoter of *RPL30* (positive control). **(M)** qPCR analysis showing fold increase in the enrichment of sXBP1 to the enhancer region of *BMPR1A* gene. n=3 per group. Data are presented as mean ± SD. *$p<0.05$, values significantly different from control IgG binding signal analyzed by unpaired Student *t* test.

FIGURE 8

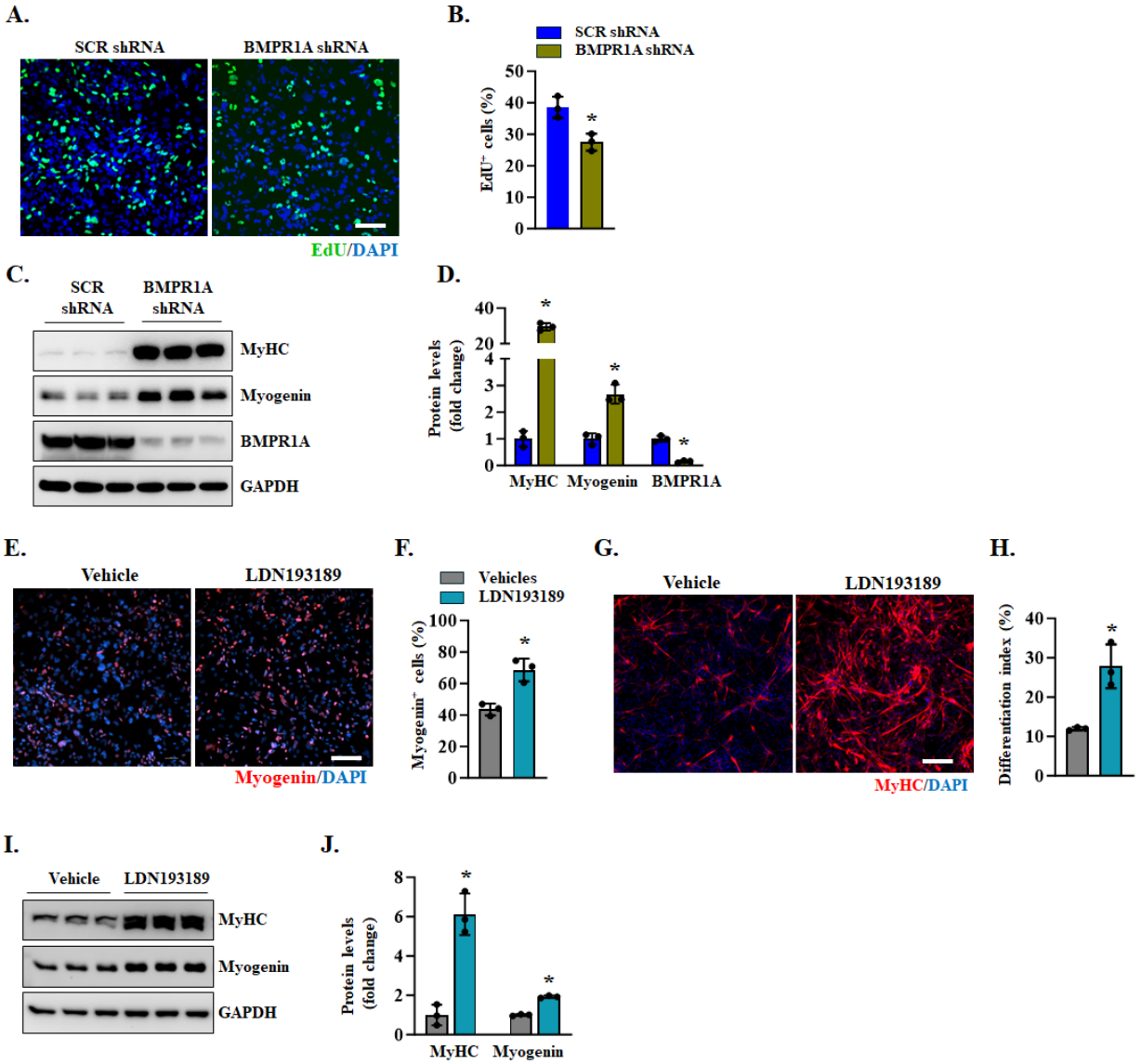

FIGURE 8. Inhibition of BMPR1A-mediated signaling suppresses proliferation and augments differentiation in RD cells. RD cells stably expressing scrambled (SCR) or BMPR1A shRNA were cultured in growth medium for 72 h, followed by EdU incorporation for 2 h. DAPI stain was used to identify nuclei. **(A)** Representative photomicrographs after EdU detection. Scale bar, 100µm. **(B)** Quantification of proportion of EdU^+ cells in SCR or BMPR1A shRNA expressing RD cultures. **(C)** Immunoblots and **(D)** densitometry analysis of levels of MyHC, myogenin, and BMPR1A protein in SCR or BMPR1A shRNA expressing RD cultures. n=3 per group. Data are presented as mean ± SD. *$p<0.05$, values significantly different from SCR shRNA expressing RD cultures analyzed by unpaired Student *t* test. RD cells were treated with 0.1µM LDN193189 (a small molecule inhibitor of BMPR1A) or vehicle alone for 72 h followed by fixation of cells and immunostaining for myogenin or MyHC protein. DAPI was used to counterstain nuclei. **(E)** Representative photomicrographs after immunostaining for myogenin. Scale bar, 100µm. **(F)** Quantification of proportion of $myogenin^+$ cells in RD cultures

treated with vehicle alone or LDN193189. **(G)** Representative photomicrographs after immunostaining for MyHC. Scale bar, 100μm. **(H)** Differentiation index in RD cultures treated with vehicle alone or LDN193189. **(I)** Immunoblots, and **(J)** densitometry analysis of levels of MyHC and myogenin protein in RD cultures treated with vehicle alone or LDN193189. n=3 per group. Data are presented as mean ± SD. *$p<0.05$, values significantly different from vehicle-treated RD cultures analyzed by unpaired Student *t* test.

FIGURE 9

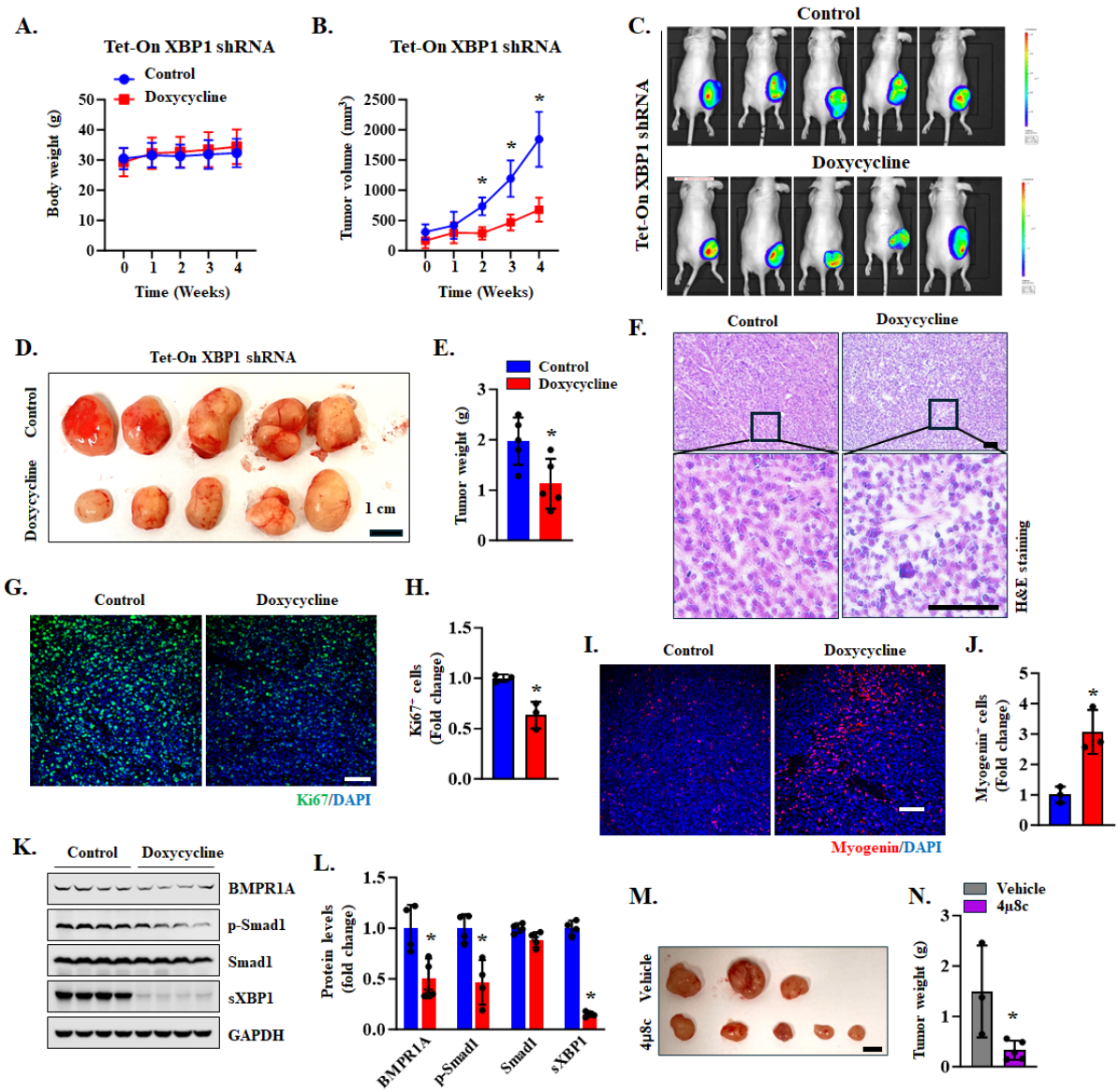

FIGURE 9. Inducible knockdown of XBP1 suppresses tumor growth in RD xenografts. (A) Body weight of mice inoculated with Tet-On XBP1 shRNA expressing RD cells fed with normal chow (control) or doxycycline-containing chow. **(B)** Average tumor volume in mice fed with normal chow or doxycycline containing chow. n=5 mice in each group. Data are presented as mean ± SD. *p<0.05, values significantly different from normal chow fed mice at indicated time points by unpaired Student *t* test. **(C)** Bioluminescence imaging showing presence RD xenograft in control and doxycycline-treated nude mice. **(D)** Images of tumors of control and doxycycline-treated group at the time of euthanizing the mice. Scale bar, 1cm. **(E)** Quantification of wet weight of tumors in control and doxycycline-treated group. n=5 mice in each group. Data are presented as mean ± SD. *p<0.05, values significantly different from control group by unpaired Student *t* test. **(F)** Representative images of tumor sections after performing H&E staining. Scale bar, 100μm. **(G)** Representative images of tumor sections after performing immunostaining for Ki67 protein. Nuclei were counterstained with DAPI. Scale bar, 100μm. **(H)** Quantification of

relative number of Ki67^{+} cells in tumor samples of control and doxycycline-treated mice. n=3 mice/group. Data are presented as mean ± SD. *p<0.05, values significantly different from control group by unpaired Student *t* test.. **(I)** Representative images of tumor sections after performing immunostaining for myogenin protein. Nuclei were counterstained with DAPI. Scale bar, 100µm. **(J)** Quantification of relative number of myogenin^{+} cells in tumor samples of control and doxycycline-treated mice. n=3 per group. Data are presented as mean ± SD. *p<0.05, values significantly different from normal chow fed mice analyzed unpaired Student *t* test. **(K)** Immunoblots and **(L)** densitometry analysis of levels of sXBP1, BMPR1A, p-Smad1, and total Smad1 in tumor samples of doxycycline-treated mice compared to control mice. n=4 mice per group. Data are presented as mean ± SD. *p<0.05, values significantly different from control group by unpaired Student *t* test **(M)** Images of RD tumors at the time of euthanizing the mice that were treated twice per week with 4µ8C (10 mg/kg body weight) or vehicle alone. Scale bar, 1cm. **(N)** Quantification of wet weight of tumors in vehicle- or 4µ8C-treated mice. n=3 (vehicle-treated) and 5 (4µ8C-treated) mice. Data are presented as mean ± SD. *p<0.05, values significantly different from control group by unpaired Student *t* test.